Journal of Nanobiotechnology

REVIEW

Open Access

The biological applications of near-infrared optical nanomaterials in atherosclerosis

Lin Shen[1,2†], Yanran Bi[1,2†], Junchao Yu[1,2†], Yi Zhong[1,2], Weiqian Chen[1,2], Zhongwei Zhao[1,2], Jiayi Ding[1,2], Gaofeng Shu[1,2], Minjiang Chen[1,2], Chenying Lu[1,2] and Jiansong Ji[1,2*]

Abstract

Purpose of review Atherosclerosis, a highly pathogenic and lethal disease, is difficult to locate accurately via conventional imaging because of its scattered and deep lesions. However, second near-infrared (NIR-II) nanomaterials show great application potential in the tracing of atherosclerotic plaques due to their excellent penetration and angiographic capabilities.

Recent findings With the development of nanotechnology, among many nanomaterials available for the visual diagnosis and treatment of cardiovascular diseases, optical nanomaterials provide strong support for various biomedical applications because of their advantages, such as noninvasive, nondestructive and molecular component imaging. Among optical nanomaterials of different wavelengths, NIR-II-range (900 ~ 1700 nm) nanomaterials have been gradually applied in the visual diagnosis and treatment of atherosclerosis and other vascular diseases because of their deep biological tissue penetration and limited background interference.

Summary This review explored in detail the prospects and challenges of the biological imaging and clinical application of NIR-II nanomaterials in treating atherosclerosis.

Keywords Cardiovascular disease, Atherosclerosis, Macrophage polarization, NIRF, NIR-II nanoparticle

†Lin Shen, Yanran Bi and Junchao Yu have Equal Contribution.

*Correspondence:
Jiansong Ji
jjstcty@wmu.edu.cn
Full list of author information is available at the end of the article

Graphical abstract

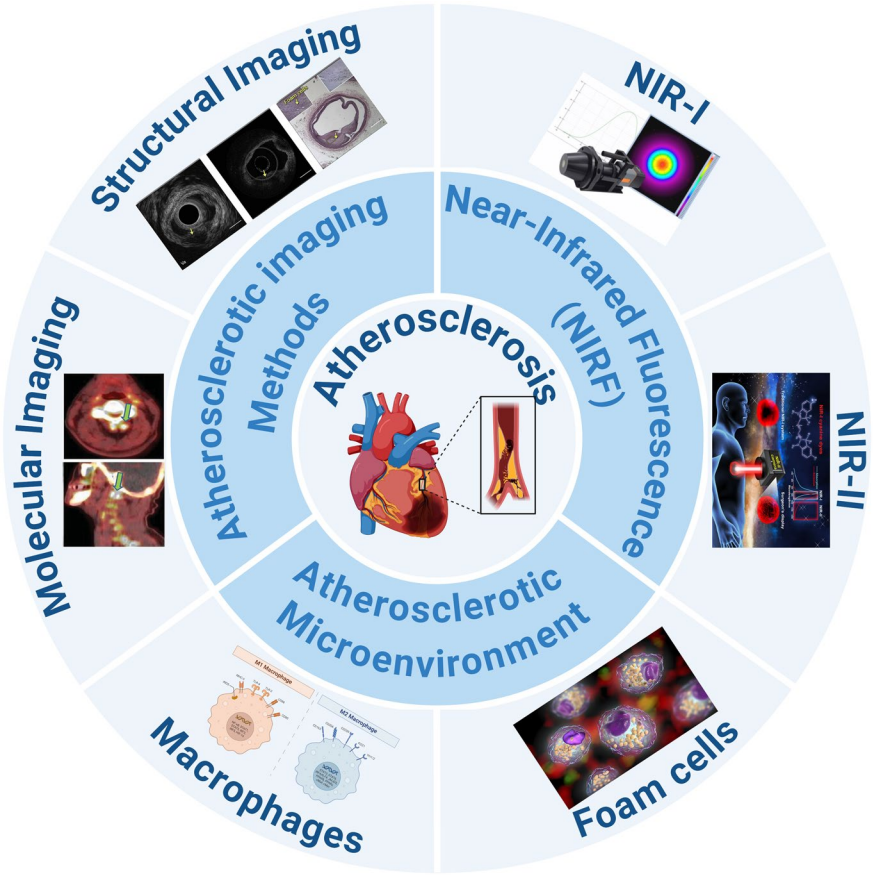

Introduction

Despite various preventive measures, cardiovascular disease (CVD) remains the leading cause of death worldwide. The number of CVD deaths worldwide increased from 12.59 million in 1990 to 20.5 million in 2021, and this number is expected to exceed 23.6 million by 2030 [1]. Atherosclerosis (AS), the main pathological basis of vascular diseases, is also difficult to clinically diagnose and treat [2–4]. Due to the deep location of the disease, existing clinical diagnostic methods cannot easily provide accurate diagnosis at an early stage. Cardiovascular and cerebrovascular adverse events caused by atherosclerotic plaque rupture are often acute and often cause irreversible damage to important organs, such as the heart and brain [5]. AS is an important cause of death and disability and seriously threatens the life safety of patients with CVD [6, 7].

With the explosive development of biomedical imaging, bio-optical imaging technology has gradually been applied to the visual diagnosis and treatment of clinical diseases because of its high precision, high efficiency and nondestructive nature [8, 9]. At present, the mainstream clinical imaging diagnostic techniques for arteriosclerosis can be divided into two main categories: noninvasive and invasive. The imaging diagnostic methods for noninvasive atherosclerosis mainly include ultrasound (US), computed tomography (CT), magnetic resonance imaging (MRI), single-photon emission computed tomography (SPECT) and positron emission tomography (PET) [10]. The imaging diagnostic methods for invasive atherosclerosis mainly include intravascular ultrasound (IVUS), optical coherence tomography (OCT) and intravascular photoacoustic imaging (IVPA) [11, 12]. Unfortunately, none of the abovementioned imaging diagnostic methods for atherosclerosis are perfect, and there are various shortcomings to some extent (Fig. 1 and Table 1).

With the advantages of being noninvasive, nonradiative and portable, ultrasound is the first choice for preliminary assessment of carotid plaque; this method can

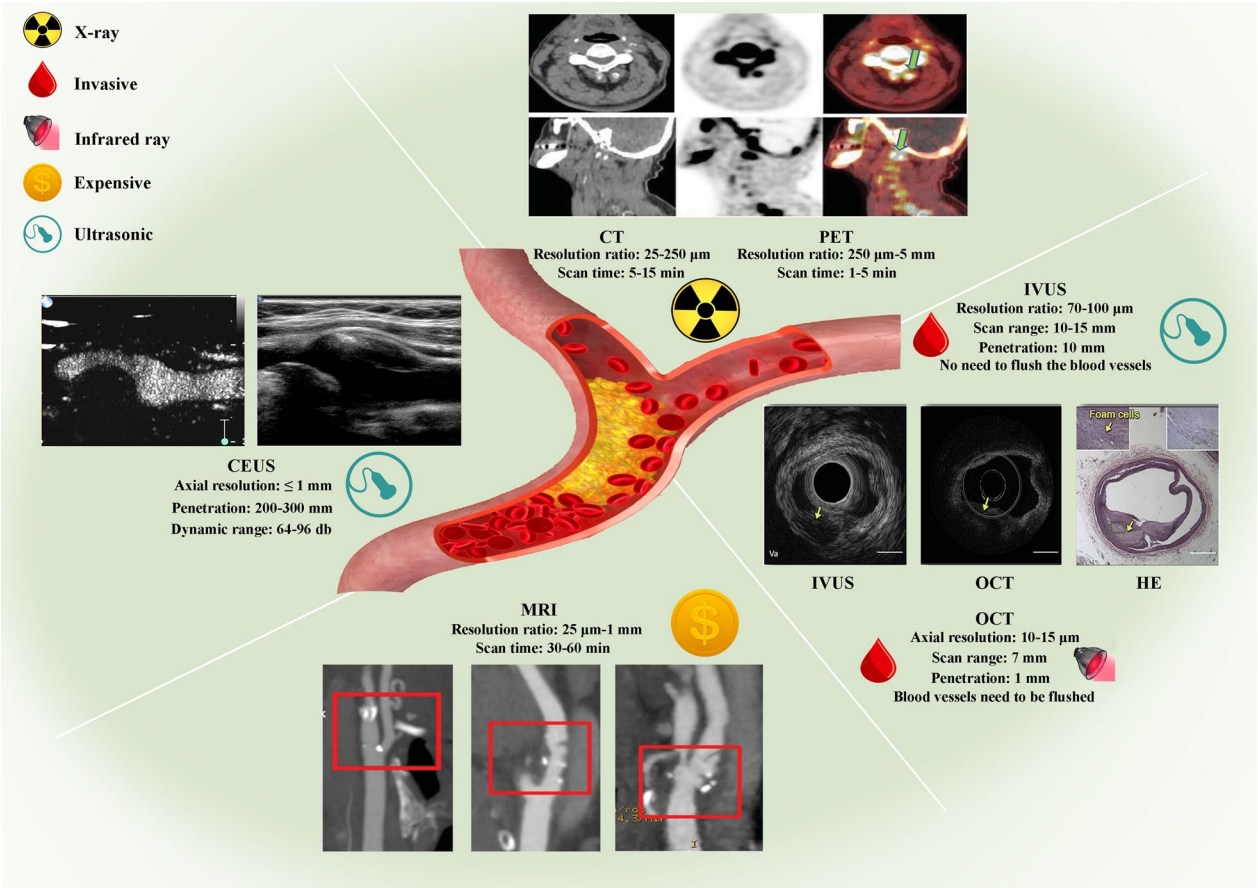

Fig. 1 Conventional imaging diagnosis of atherosclerosis. Noninvasive imaging techniques for atherosclerotic plaques include CT, PET, MRI and CEUS, while the main invasive imaging techniques are OCT and IVUS. This figure shows the sensitivity, relative costs, resolution range and scan time range. MRI, CT and PET images were obtained from ref. [10]; CEUS images from ref. [127]; and IVUS and OCT images from ref. [128]. All of the imaging devices mentioned above have been approved by the FDA

clearly show the location and size of plaque and the degree of narrowing of blood vessels [13]. However, the irregular surface of ulcerated plaques weakens edge echoes, and the high echo shadow of calcified plaques covers the local visual field, which ultimately limits the accurate screening of ulcerated plaques and calcified plaques by ultrasound [14]. Moreover, CT, another noninvasive imaging diagnostic method for atherosclerosis with good spatial resolution, can assess lumen stenosis and characterize high-risk plaque features such as positive remodeling, calcification, and ulceration [15]. However, CT is unable to identify the soft tissue components of plaques, which prevents CT from accurately differentiating stable atherosclerotic plaque lesions from acute plaque bleeding or thrombosis [16]. Unlike ultrasound and CT, MRI is an effective way to quantify the composition of arterial plaque [17]. MRI provides excellent soft tissue contrast, avoids ionizing radiation and is not affected by artifacts such as calcification [17]. However, MRI has limitations, such as long scan times, contraindications, the need for contrast agents, and expensive technology [8]. PET and SPECT use radionuclides to label intermediates involved in atherosclerosis for imaging [18, 19]. Compared with other imaging methods, these methods have irreplaceable advantages in quantifying the main components of atherosclerotic plaques and determining changes in metabolic function [19]. PET images have higher resolution and are more widely used than SPECT images. At present, positron emission tomography (PET) is widely used in clinical studies of carotid plaque characteristics, mainly involving the use of the ^{18}F-fluorodeoxyglucose (^{18}F-FDG) tracer, which can aggregate in metabolically active inflammatory macrophages [20]. In carotid atherosclerosis, increased uptake of.^{18}F-FDG is a marker of plaque glucose metabolism and inflammation and is strongly correlated with endometrial macrophage infiltration, suggesting plaque vulnerability [20]. However, the high cost and ionizing radiation of radionuclides limit the wide application of PET and SPECT in atherosclerosis imaging [21].

Table 1 Comparison of traditional imaging methods for atherosclerotic plaques

	Imaging method		Advantages	Disadvantages
Non-invasive imaging diagnostic methods	US	CDFI	(1) Widely used in the detection of vascular lesions in clinical patients (2) Observe the level and structure of vascular wall (3) Preliminary judgement of the size, classification and stability of atherosclerotic plaque	(1) Unable to provide a more comprehensive morphology of diseased blood vessels (2) The operation is complicated (3) The acquisition of pathological information is also affected by the proficiency of operation
		CEUS	(1) It can accurately identify potentially vulnerable plaques (2) It can reflect the neovascularization in plaque (3) To predict the occurrence of acute cardio-cerebrovascular events	(1) It is highly dependent on the skill and level of the operator (2) The acoustic shadow area behind the calcified plaque could not be detected (3) All kinds of ultrasonic artifacts may affect the display of plaque images
	CT		(1) Has good spatial resolution (2) Highly sensitive to stenotic plaques (3) Plaque morphology is good (4) High availability	(1) It is impossible to accurately identify the different components within the plaque, such as fiber cap, lipid core and so on (2) There are artifacts in CT spiral scan, which may lead to poor spatial resolution, partial volume effect, and overlapping interference in density values (3) CT angiography should be injected intravenously with iodine as contrast enhancer, but should not be used in patients with iodine allergy (4) The dose of ionizing radiation is high and it is harmful to human body
	MRI		(1) Good display of morphology and function (2) Non-ionizing radiation (3) High spatial resolution (4) The resolution of soft tissue density is high, and the blood (5) Vessel wall and surrounding tissue can be clearly displayed (6) Accurate evaluation of the shape and composition of AS plaques (7) Early prediction of plaque rupture	(1) In the process of detection, it is easy to produce motion artifacts due to vascular pulse and respiration (2) High cost (3) Large dose of contrast agent
	PET/SPECT		(1) Anatomical and metabolic display is excellent (2) The different stages of atherosclerotic plaque can be evaluated dynamically (3) The structure and cellular components of plaques can be identified (4) It can predict the occurrence of thrombotic events (5) Risk stratification of patients with AS can be performed	(1) Limited availability (2) High cost (3) High ionizing radiation
Invasive imaging diagnostic methods	IVUS		(1) Positive remodeling of blood vessels in plaques can be observed (2) Measure plaque burden (3) Reflect the morphological characteristics of plaque	(1) Insufficient detailed analysis of plaque composition characteristics (2) The display of the plaque site is greatly affected by the angle of the sound wave (3) Great dependence on the operator (4) Lack of specificity for calcification and intracavicular hemorrhage
	OCT		(1) High resolution (axial 10 μm, lateral 25 μm), (2) Can identify the status of arterial blood wall and vascular lumen; (3) It can show the characteristics of three kinds of plaques: fibrous plaque, fibrous calcified plaque and lipid-rich plaque; (4) Identify atherosclerotic vulnerable plaques by observing plaque microstructure and quantitatively analyzing macrophages	(1) It is an invasive diagnosis (2) Its penetration is limited (3) Plaque load cannot be assessed (4) Infrared light is heavily affected by blood, and blood vessels need to be flushed before imaging (5) High requirements for contrast media and artifacts
	IVPA		(1) The morphology and composition of plaques can be shown simultaneously (2) The identification of lipid components is highly specific (3) Both ultrasonic and optical imaging advantages	Blood in the blood vessel can significantly reduce the light absorption intensity of the blood vessel wall and reduce the imaging quality

CDFI color doppler flow imaging, *CEUS* contrast-enhanced ultrasound, *CT* computed tomography, MRI magnetic resonance imaging, *PET* positron emission tomography, *SPECT* single photon emission computed tomography, *IVUS* intravascular ultrasound, *OCT* optical coherence tomography, *IVPA* intravascular photoacoustic imaging

IVUS is an invasive technique performed using ultrasonic reflection amplitude imaging and is considered the gold standard for diagnosing atherosclerotic plaques [22]. IVUS can determine the nature of atherosclerosis based on the echocardiographic characteristics of the plaque and can accurately determine the narrowing of the lumen and the thickness of the blood vessel wall [22]. Its main advantage is that it allows deep tissue penetration and can provide cross-sectional images of the entire vessel wall; this approach is the most commonly used intracavity coronary imaging technique today [22, 23]. However, IVUS has difficulty accurately displaying the fine structure and composition of vulnerable plaques due to its low spatial resolution and interference from acoustic shadows of calcium deposits [23]. OCT, an endovascular imaging technology with the highest resolution and most accurate evaluation of coronary artery AS plaques, mainly images normal blood vessels and plaques through optical signal attenuation. Compared with IVUS, OCT can accurately distinguish fibrous plaque, calcified plaque, lipid plaque and thrombus and has far-reaching guiding significance for the preoperative evaluation of stent implantation, intraoperative plaque status monitoring, postoperative follow-up and drug treatment evaluation [24]. However, due to the limitations of light penetration, it is difficult for OCT to monitor the atherosclerotic necrotic core in the deep layer of the blood vessel wall, so it is unable to evaluate the plaque load. [25]. In addition, OCT is highly susceptible to blood interference and requires a higher concentration of contrast agents [26]. As a typical application of endoscopic photoacoustic tomography (EPAT), IVPA offers the advantages of both ultrasonic depth detection and optical high-resolution imaging. Compared with IVUS, IVPA exploits the difference in the light absorption ability of different tissue components, and its contrast is greater than that of IVUS [27]. IVPA can be used to effectively distinguish lipids from calcified plaques in blood vessel walls and reveal the fine structure of plaques; thus, IVPA is a promising research method. [28]. However, because blood in vivo is a type of strongly scattering tissue that can significantly reduce the light absorption intensity of the vascular wall and affect the image quality of vascular and plaque images, the current stage of IVPA is still in the preclinical stage [27, 28].

AS formation is a very complex process, and optical technology is among the above traditional clinical biomedical imaging techniques because of its ability to accurately track complex tissue components in atherosclerotic plaques [29]. In particular, near-infrared fluorescence (NIRF) imaging not only has the rapid feedback, high resolution and noninvasive characteristics of conventional optical imaging but also has the least amount of tissue interference in the NIR window; therefore, it has been gradually applied to in vivo imaging with high signal-to-noise ratios (SNRs) [30, 31]. Interestingly, because NIR-II (1000 ~ 1300 nm) has lower spontaneous background fluorescence, deeper tissue penetration and a higher SNR than does NIR-I (700 ~ 900 nm), it has become an effective means of real-time monitoring of the progression of vascular diseases in the field of NIRF [32, 33].

Thus, through this review, we systematically summarize the latest progress in the application of NIR-II fluorescent nanomaterials in atherosclerotic biological imaging of highly pathogenic vascular diseases and analyze the challenges and prospects of their clinical application.

Imaging of atherosclerotic plaques

Structural feature imaging of atherosclerotic plaques

Vulnerable atherosclerotic plaque rupture is the main cause of acute cardio-cerebrovascular events [34]. Therefore, the structural feature of lumen stenosis is regarded as the main assessment index of vascular risk in traditional clinical atherosclerotic imaging [34]. The imaging methods used to explore the anatomical characteristics of plaques include both invasive and noninvasive imaging techniques. Among the various noninvasive examination techniques, CT coronary angiography (CTA) can accurately identify the risk characteristics of unstable atherosclerotic plaques, such as positive remodeling, low-density plaque and punctate calcification; thus, this technique is effective at predicting acute cardiovascular events [35]. Invasive examination methods mainly include OCT, IVUS and IVUS virtual histology (IVUS-VH). Among these methods, IVUS is the most effective method for detecting unstable atherosclerotic plaques and is widely used in clinical studies to identify and predict potential lesions causing acute cardiovascular events [36]. Significantly, IVUS can clearly identify vascular positive remodeling and thin-cap fibroatheroma (TCFA), which are usually mild on angiography [37, 38].

As a new intracoronary imaging technique after IVUS, OCT can accurately display the microstructure and components of coronary artery walls, such as the TCFA, fat, macrophages, thrombi and calcified nodules. Compared with IVUS, the extremely high resolution of OCT images has made it increasingly important to evaluate vulnerable plaques and guide stent implantation, especially in the diagnosis and treatment of acute coronary syndrome (ACS). OCT can also be used to evaluate the arterial wall response after percutaneous coronary intervention (PCI) [39]. A multicenter Centro per la Lotta contro l'Infarto-Optimization of Percutaneous Coronary Intervention (CLI-OPCI) study conducted in 2012 showed that, compared with PCI therapy guided by radiography alone, OCT-guided PCI therapy could significantly

improve the prognosis of patients [38]. Subsequently, in the 2013 European College of Cardiology Guidelines for the Management of Stable Coronary Heart Disease, OCT was listed as a Class IIb recommendation (evidence level B) for evaluating lesion characteristics and optimizing stent implantation, and the overall level of evidence was equivalent to that of IVUS [39]. In 2014, the European Society of Cardiology/European Association of Cardiothoracic Surgeons (ESC/EACTS) myocardial revascularization guidelines upgraded OCT's recommendation for optimized PCI to the Class IIa equivalent of IVUS [40]. The ILUMIEN I study published in 2015 showed that OCT examination before and/or after PCI can affect the intervention strategy used for patients [41]. The results of the ILUMIEN II study showed that OCT is not inferior to IVUS for guiding stent expansion [42]. With the continuous update of OCT technology and the publication of additional prospective research data, the use of OCT in the field of diagnosing and treating CHD will further increase.

Although clinical imaging methods for structural features provide unprecedented morphological detail, the potential for accurate identification of plaque grade is very limited. For example, the assessment of atherosclerotic plaques by CTA and magnetic resonance angiography (MRA) mainly depends on the degree of lumen stenosis, but the main determinant of acute clinical events is the biological composition of the atherosclerotic plaque microenvironment, not arterial stenosis [43]. The ability of OCT to distinguish between fat accumulation in non-necrotizing cells and necrotic lipid cores is unclear, which limits its ability to precisely diagnose advanced and ruptured plaques [44]. Additionally, the deterioration of atherosclerotic plaques involves complex interactions among the structural, cellular and molecular components of vessel walls, so microscopic structural imaging of artery walls alone cannot fully reveal the progression of CVD [45, 46].

Molecular imaging of atherosclerotic plaques

Because atherosclerosis is the biological consequence of the accumulation of inflammatory cells and lipid oxides in the blood vessel wall, molecular imaging, as a supplementary method of structural feature imaging, monitors the changes in molecular composition during the process of deterioration in atherosclerosis and helps to determine the mechanism of atherosclerosis progression and complications [47].

At present, there are many molecular imaging methods for the clinical diagnosis of atherosclerotic plaques [48, 49]. MRI was used to identify vulnerable areas of coronary plaques by non-contrast T1-weighted imaging, while PET was used to assess vascular inflammation and microcalcification at vulnerable plaques by ^{18}F-FDG and ^{18}F-sodium fluoride (^{18}F-NaF), respectively [50, 51]. Interestingly, ^{18}F-FDG PET imaging demonstrated an advantage in detecting inflammatory cells (macrophages) in plaques in large arteries (carotid arteries, iliac arteries, aorta), whereas.^{18}F-NaF PET imaging was primarily good at revealing calcified plaques in coronary arteries, which also provides a new strategy for specific diagnosis and treatment of the atherosclerotic plaque microenvironment [52].

^{18}F-FDG, a glucose analog, can be taken up by inflammatory macrophages with active glycolytic metabolism in plaques and is a reliable PET tracer for atherosclerosis treatment [53]. ^{18}F-FDG-6-phosphate, which is taken up and phosphorylated by macrophages, cannot be further degraded via the glycolytic pathway and gradually accumulates with inflammatory macrophages in plaques, thus reflecting the degree of plaque inflammation and the macrophage content [53]. Interestingly, many studies have confirmed that aortic ^{18}F-FDG uptake not only is significantly related to coronary artery calcification in patients with CHD but can also independently predict the occurrence of acute cardio-cerebrovascular events via ^{18}F-FDG PET imaging [54–56]. The multimodal combination of.^{18}F-FDG PET with CT or MRI imaging systems will also provide additional prognostic information for atherosclerotic plaque imaging in addition to risk factor assessment and structural imaging data [57, 58]. However, the disadvantages of these diagnostic methods, such as complex operation and high radiation, limit their wide application in the clinic [59].

Near-infrared fluorescence imaging system for atherosclerosis

Because of its benefits, such as ease of use, small equipment size, high sensitivity, good temporal resolution and low self-fluorescence effect, NIRF imaging has garnered much interest in the field of molecular imaging [60, 61]. After targeted modification, nanoparticles or dye molecules with fluorescence emission can target the focus for fixed-point imaging and detection, which is extremely important for the diagnosis of AS [62].

In biological applications, near-infrared (700 ~ 1700 nm) fluorescence imaging technology is becoming increasingly important [63, 64]. There are several drawbacks to fluorescence imaging, including the use of visible light (400 ~ 700 nm) and classic near-infrared light (NIR, 700 ~ 900 nm) wavelengths, as well as the significant autofluorescence of biological tissue and limited tissue penetration [65]. Recent research has demonstrated

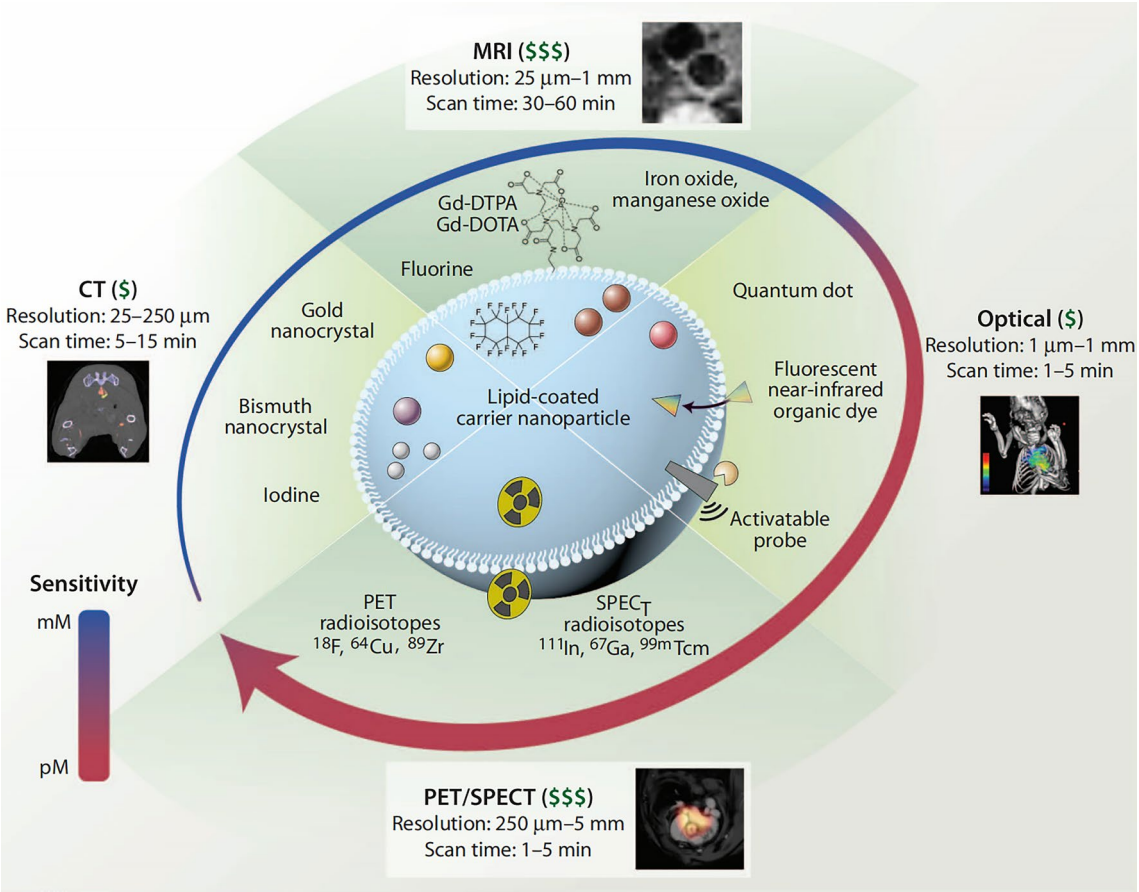

Fig. 2 Imaging with nanoparticles and related diagnostic techniques. To identify nanoparticles in plaque cells using CT, MRI, optical techniques, or nuclear imaging, including PET and SPECT, a range of imaging agents can be used. The relative price, sensitivity, scan time range, and resolution range are indicators. This figure was reproduced from ref. [61]

that biomedical imaging in the second near-infrared region (NIR-II, 1000 ~ 1300 nm) can significantly improve the spatiotemporal resolution (approximately 20 ms and approximately 25 mm) over that of NIR-I. These benefits come from reduced scattering, minimal tissue absorption, and minimal self-fluorescence effects [66].

(See figure on next page.)

Fig. 3 Differences between the NIR-I and NIR-II in biological imaging. **A** Diagram showing the imaging setup in which Hongjie Dai's team used silicon and InGaAs cameras for the simultaneous detection of NIR-I and NIR-II photons. Adjustable magnifications were achieved using a series of zoomable lenses. Reproduced from ref. [62]. **B** Sensitivity curves for common cameras based on sensors made of silicon (Si), mercury cadmium telluride (HgCdTe), or indium gallium arsenide (InGaAs). HgCdTe is more sensitive at longer wavelengths, while Si and InGaAs cameras are sensitive inside the first and second near-infrared windows, respectively. copied from the source. Reproduced from ref. [71]. **C** The effective attenuation coefficient (on a log scale) against wavelength plots indicated that the first (pink shaded area) or second (gray shaded area) near-infrared window had the lowest absorption and scattering from skin, fatty tissue, deoxygenated blood, and oxygenated blood. copied from the source. Reproduced from ref. [73]. **D** UV absorption and fluorescence emission spectra of Ag_2Se QDs coated with PEG and C18-PMH. The NIR-II fluorescence image of the C18-PMH-PEG-Ag_2Se QDs and the corresponding scheme are shown in the inset. Reproduced from ref. [82]. **E** Emotion of in vivo fluorescence images of mice following intravenous injection of NIR-II Ag_2Se QDs (left) or NIR-I ICG (right) as a reference. Reproduced from ref. [82]. **F** Taken from reference live mice, bright field (left) and fluorescence (center) images were obtained by injecting PEGylated Ag_2S QDs (NIR-II, 1 mg/mL, 50 mL) subcutaneously into the right footpad. Cross-sectional fluorescence intensity profiles (right) showing the results of QD injection in mice are shown along the red dashed bars. The red-dashed curves represent Gaussian fits to the profiles. Reproduced from ref. [83]. **G** Live mice were subjected to bright field (left) and fluorescence (center) imaging via the subcutaneous injection of ICG (NIR-I, 1 mg/mL, 50 mL) into the left footpad. Cross-sectional fluorescence intensity profiles (right) of an ICG-injected mouse shown along red dashed bars. The red-dashed curves represent Gaussian fits to the profiles. Reproduced from ref. [83]

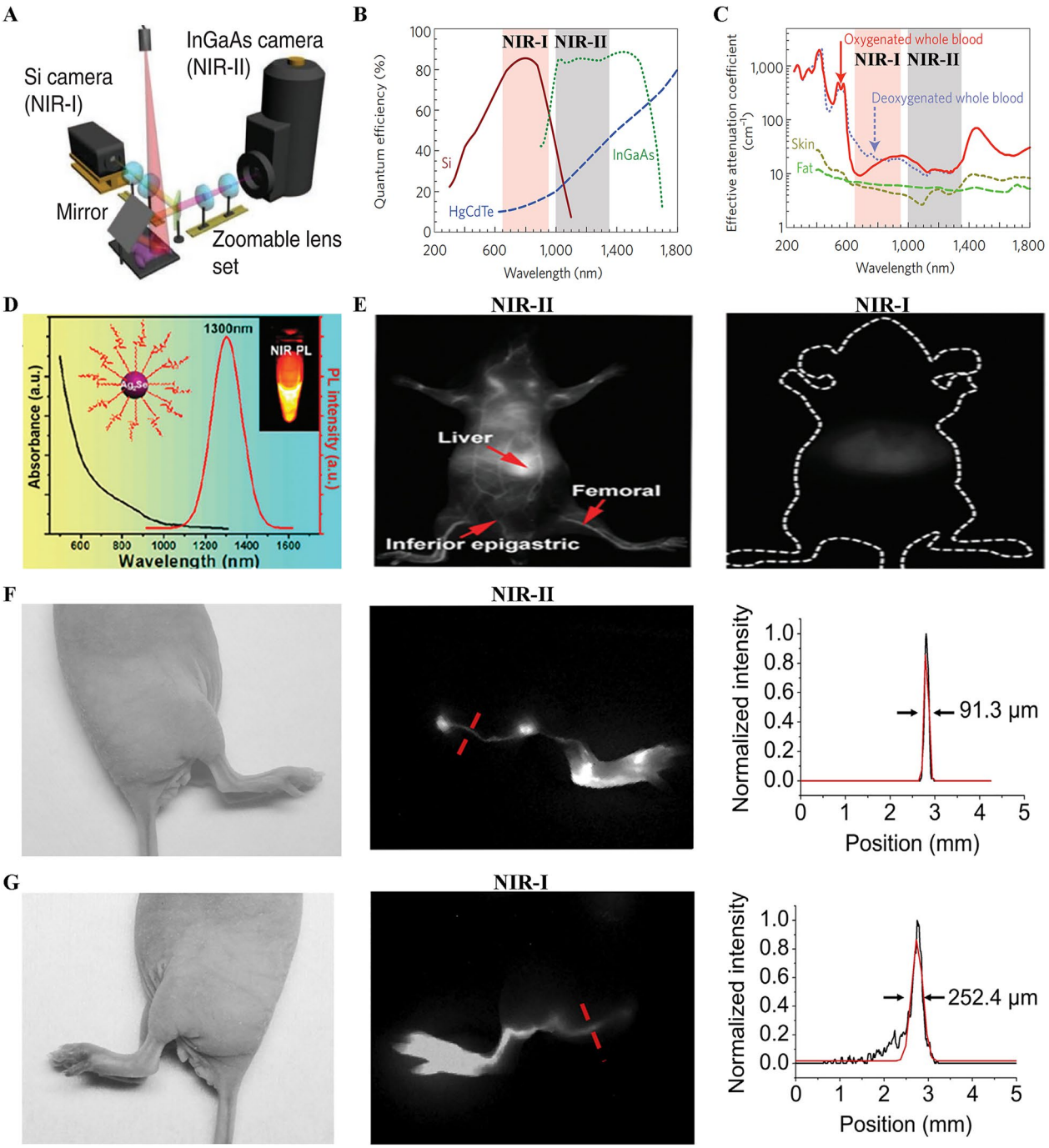

Fig. 3 (See legend on previous page.)

Before the emergence of NIR-II imaging, although traditional cardiovascular imaging techniques such as CT (0.5 ~ 0.625 mm, 83 ~ 135 ms), MRI (2 mm, 50 ms), PET (10 mm, 5 min) and SPECT (15 mm, 15 min) had certain advantages in spatial resolution, the temporal resolution was far below the need for the diagnosis of microatherosclerotic plaques [58]. Because different atherosclerotic plaque types need to be distinguished by analyzing temporal and spatial speckle pattern fluctuations, the time constant of plaque decorrelation is significantly different among vulnerable plaques ($\tau = 40$ ms, stable plaques ($\tau = 400$ ms) and normal aortas ($\tau = 500$ ms), which shows that NIR-II imaging seems to be the method with the best spatiotemporal resolution for plaque diagnosis [67].

Table 2 Comparison of NIR-II fluorescent materials

Types	Classification	NIR-II fluorescent materials	λexc/nm	λem/nm	Quantum yield/%	Application
Organic NIR—II fluorescent probe	BBTD	FM1210-NPs	980	1210	0.04	In vivo imaging of tumor and vascular system
		BBTD-1302NPs	942	1302	2.4	Photothermal therapy of tumor
		IR-FP8P	748	1040	0.6	Angiography of hind limbs in mice
		SA-TTB-PEG_{1000}	808	1050	10.3	Diagnosis and treatment of vascular diseases
		CH-4T-FBS	808	1050	0.1	Imaging of vascular system and lymph nodes in hind limbs
		Q4-1	808	1100	0.2	Organ imaging in mice
	Cyanine	IR-783@BSA	785	1433	21.2	Tumor imaging
		NIRII-RTs	977	1008	2.03	Real time monitoring of ATP content in liver
		Fd-1080J-aggregate	1360	1370	0.06	To monitor the dynamic changes of carotid artery and evaluate the efficacy of antihypertensive drugs
		ICG	782	880–1450	0.9	Vascular system and hindlimb imaging
	BODIPY	SWIR-WAZABY-01	638	720–1200	2.5	Tumor imaging
		NJ-1060	808	1060	1	Cerebral angiography
	Conjugated polymer	m-PBTQ4F	808	850–1400	3.2	Imaging of vascular system of skull tumor in mice
		PDFT1032	808	1032	/	Angiography
		pDA-PEG	808	1047	1.7	Ultrafast near infrared imaging of arterial blood flow
Inorganic NIR—II fluorescent probe	Rare earth nanomaterials	RENPs@Lips	800	1064/1345	7.90/4.10	In situ tumor angiography
		Y_2O_3:Yb, Er	980	1550	/	Organ imaging
		$NaYF_4$:Yb:Er@$NaYF_4$	980	1525	/	Early detection of tumor
		$NaYF_4$:Yb@$NaYF_4$:Nd	808	1530	/	High resolution tracking and imaging of tumors
	Quantum dot	9T-GQDs	1064	/	16.67	Image guided cancer treatment
		Zn-doped PbS-PEG	1550	1630	50	High resolution fluorescence imaging of cerebral vessels
		Ag_2S-6PEG	808	1200	15.5	Tumor imaging
		Ag_2S-PEG	808	1200	16	Lymphatic drainage imaging, hematography
		Ag_2S-SiO_2	785	1135	22.7	Tumor imaging
	Inert metal nanomaterials	RNase-A@AuNCs	808	1050	1.9	Colorectal cancer imaging
		$Au_{25}(SG)_{18}$	808	1050	0.27	Intraoperative fluorescence navigation of bone tissue
		AuNCs-Pt	808	945/1035	0.04	Integration of diagnosis and treatment to eliminate high risk deep tumor
	Single walled carbon nanotubes	Chiral SWCNTs	725	850/1350	/	Angiography
		SWCNTs-mPEG	808	1100–1400	0.1	Tumor imaging
		LV SWCNTs	808	1200–1800	0.01	High power cerebral angiography
		SWCNTs-DSPE-mPEG	808	1100–1700	0.1	Video rate in vivo imaging
		SWCNTs-cholate	808	900–1500	0.4	In vivo tumor angiography

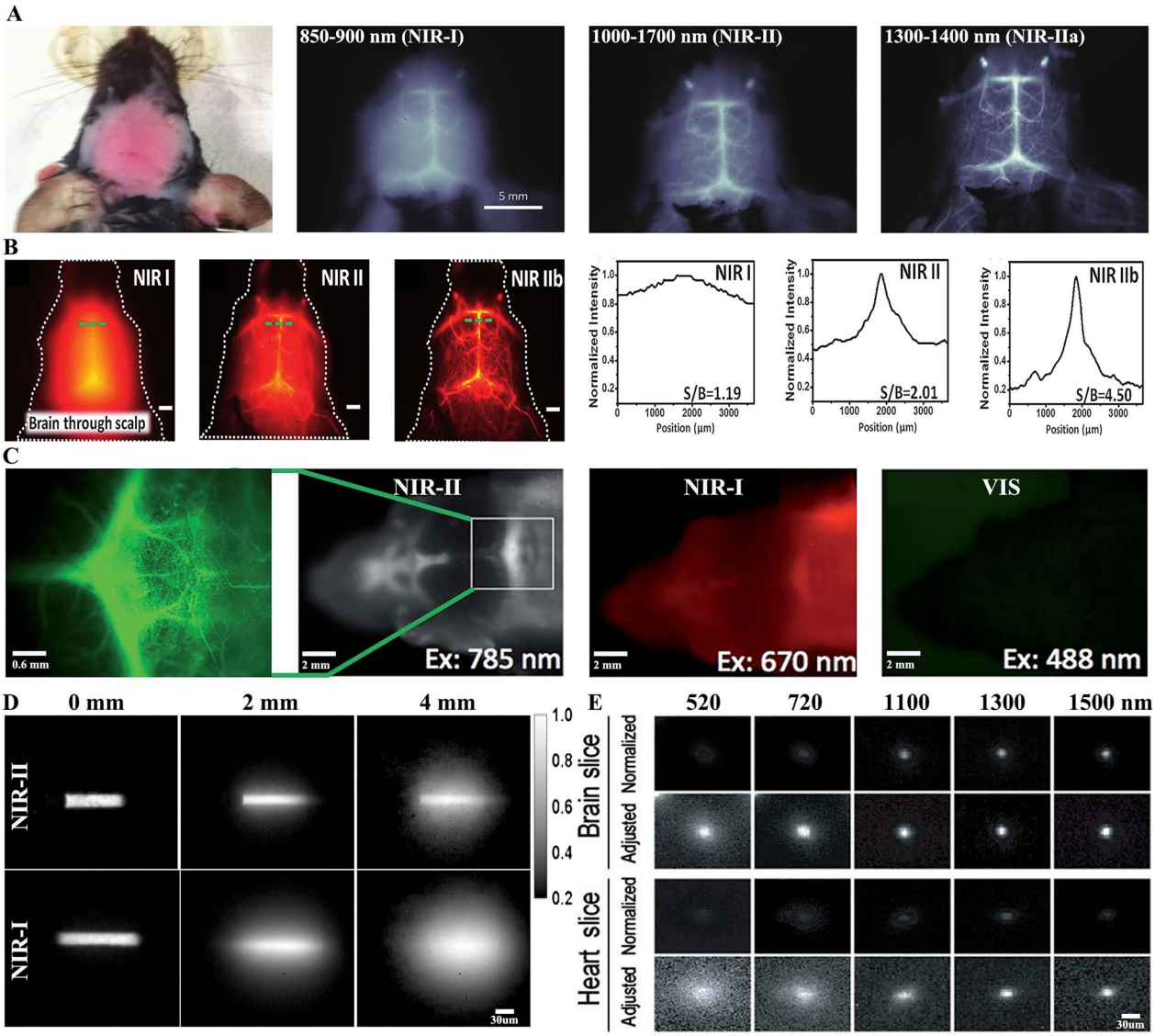

Fig. 4 Comparison of in vivo cerebrovascular imaging between the NIR-I and NIR-II groups of mice. **A** In vivo mouse brain imaging of the NIR subregions (NIR-I, NIR-II, and NIR-IIa) using SWNT-IRDye800. Reproduced from ref. [87]. **B** Fluorescence images, together with the associated SBR analysis, of the cerebrovasculature in the NIR-I, NIR-IIa and NIR-IIb areas of mice (n = 2) that did not undergo craniotomy. 2 mm scale bars. Reproduced from ref. [88]. **C** The VIS (520 nm), NIR-I (720 nm), and NIR-II (1300 nm) fluorescence images of mouse heads are displayed by fluorescence angiography; the excitation wavelengths are 488 nm, 670 nm, and 785 nm, respectively. Reproduced from ref. [90, 91]. **D** Fluorescence images of the capillaries of ICG (NIR I) and SWNTs (NIR II) in Intralipid® stimulated at 785 nm at depths of 0, 3, and 5 mm. Compared to the ICG sample, the SWNT sample exhibited reduced feature spread. The scale bar is 1.5 cm. Reproduced from ref. [90, 91]. **E** QD-doped porous beads (15 mm in diameter) and their transit into tissue are shown in microscopy images. The brain and heart slices had thicknesses of 100 and 200 mm, respectively. The fluorescence intensities in the normalized images are displayed in relation to the intensities when tissue slices were not present. Images with adjustments display the fluorescence intensities normalized to the intensity from peak to peak. Reproduced from ref. [90, 91]

Nanomaterial imaging system for atherosclerosis

Atherosclerosis is a complex chronic inflammatory disease, and novel tools are needed to identify and inhibit atherosclerotic inflammatory cells with high accuracy. Biological nanomaterials can be loaded with high-dose contrast agents or therapeutic drugs to efficiently deliver drugs to plaques by exploiting long-term circulation and actively targeting plaques in the body [68]. Therefore, nanoimaging is suitable for treating diseases such as atherosclerosis, cancer, myocardial infarction, aortic aneurysm, and diabetes and is expected to enable non-invasive imaging in vivo to accurately determine the

clinical results of patients and formulate effective treatment plans.

Nanomaterials have been used in optical imaging, MRI, CT and multimodal imaging for AS detection (Fig. 2) [69]. Optical imaging based on nanomaterials can detect abnormal changes at the cellular or molecular level earlier than can other methods, providing more accurate supplementary information for the diagnosis of AS and facilitating the early detection, screening, evaluation, and image-guided treatment of AS lesions.

Application of NIR-I and NIR-II in biological imaging

Dai et al. created NIR-I and NIR-II imaging systems for the first time, as shown in Fig. 3A. [70] Alloys of semiconductors for NIR-II fluorescence imaging and camera materials such as InGaAs and HgCdTe can be used. At wavelengths longer than 1700 nm, the HgCdTe detector exhibits the highest sensitivity; however, its overall quantum efficiency is quite low. Conversely, inside the NIR-II window, the InGaAs detector exhibited a high quantum efficiency of up to 90% (Fig. 3B) [71]. A novel visual detection method in vivo is fluorescence imaging technology, which is highly sensitive and has high temporal and spatial resolution. Traditional near-infrared fluorescence imaging is mainly focused on superficial lesions; therefore, surgery is often needed to expose the tumor area. When light penetrates a biological tissue, it attenuates due to the absorption and scattering of the tissue [72]. In the near-infrared region (700 ~ 1700 nm), the attenuation coefficient of biological tissue remains relatively low but is almost 100 times greater than that in the ultraviolet and visible regions (Fig. 3C) [73].

NIR-II imaging results in a greater SNR, deeper tissue penetration, and lower spontaneous background fluorescence than NIR-I imaging. NIR-II fluorescence imaging can therefore aid in the precise identification of deep-seated illnesses. NIR-II fluorescence imaging is based on the NIR-II fluorescent probe. Many organic and inorganic materials have been used to create a variety of NIR-II fluorescence probes. These materials include conjugated polymers, organic nanoparticles derived from small-molecule dyes, organic small-molecule dyes, quantum dots, rare-earth doped nanoparticles, and single-walled carbon nanotubes (Table 2) [63, 74–77].

Among the reported candidate nanomaterials for NIR-II fluorescence imaging, sulfur-containing silver quantum dots (QDs) and SWCNTs are the most promising [78–81]. The photochemical stability of the chalcogenide silver QDs is 10 ~ 1000 times greater than that of the NIR-I dye ICG. In addition, the QD brightness is 10 ~ 100 times greater than the ICG brightness. Compared with those of ICG, Ag_2S and Ag_2SeQD with NIR-II fluorescence can obtain high-resolution images with deep whole-body vascular networks as low as ~ 24 mm and 50 ms (Fig. 3 D, E) [82]. Using Ag_2S quantum dots as an imaging agent, NIR-II fluorescence imaging can clearly reveal blood vessels and lymphatic vessels (Fig. 3 F, G) [83]. In contrast, the NIR-I fluorescence signal is very weak, and the blood vessels and lymphatic vessels are not clearly displayed [82–84].

Single-walled carbon nanotubes (SWCNTs) in the NIR-II window are known for their extended blood circulation and high light stability. Welsher et al. established the standard for in vivo NIR-II fluorescence imaging by employing SWCNTs for the first time to image tumor vessels in mice through intact skin [85]. This work inspired numerous studies investigating NIR-I-to-NIR-II fluorescence imaging in the biomedical domain [86]. Nevertheless, because of insufficient imaging speed and spatial resolution, current brain imaging technology obviously limits the resolution of middle and small blood vessel images and real-time monitoring of dynamic blood flow in the blood vessels of the brain. To solve this problem, SWCNTs with NIR-IIa (1300 ~ 1400 nm, Fig. 4A) [86] and NIR-IIb (1500 ~ 1700 nm, Fig. 4B) fluorescence [87] have been used for cerebrovascular imaging; these materials can penetrate the entire scalp and skull and noninvasively provide cerebrovascular ultrahigh spatial resolution. More importantly, NIR-IIb fluorescence imaging has a high signal-to-background ratio (SBR) of 4.50 and can simultaneously measure the blood flow velocity in multiple blood vessels at a high speed of 4.6 fps, which is far better than the speed of traditional NIR-IIa and NIR-I fluorescence imaging.

At present, there are two clinically approved NIR-I dyes, indocyanine green (ICG) and methylene blue (MB). They have been widely used to minimize surgical risk and improve the cure rate [88]. However, the low light stability and tissue penetration of NIR-1 dye greatly limit its application in deep blood vessel visualization. Some studies have used ICG and SWCNTs to simulate the penetration depth of near-infrared fluorescence at different wavelengths in the human body. They discovered that, compared with traditional NIR-I, NIR-II can offer greater image contrast at a greater penetration depth. (Fig. 4C-E) [89, 90].

There is a growing range of available NIR-II fluorescent materials. However, the development of NIR-II fluorescent materials has hit a roadblock because of the lack of good water solubility, stability, fluorescence efficiency, and biocompatibility. Solutions to these issues are highly desirable for future development in the field of NIR-II fluorescence imaging. The advancement of fluorescence imaging technology greatly depends on the creation of new NIR-II fluorescent materials with high

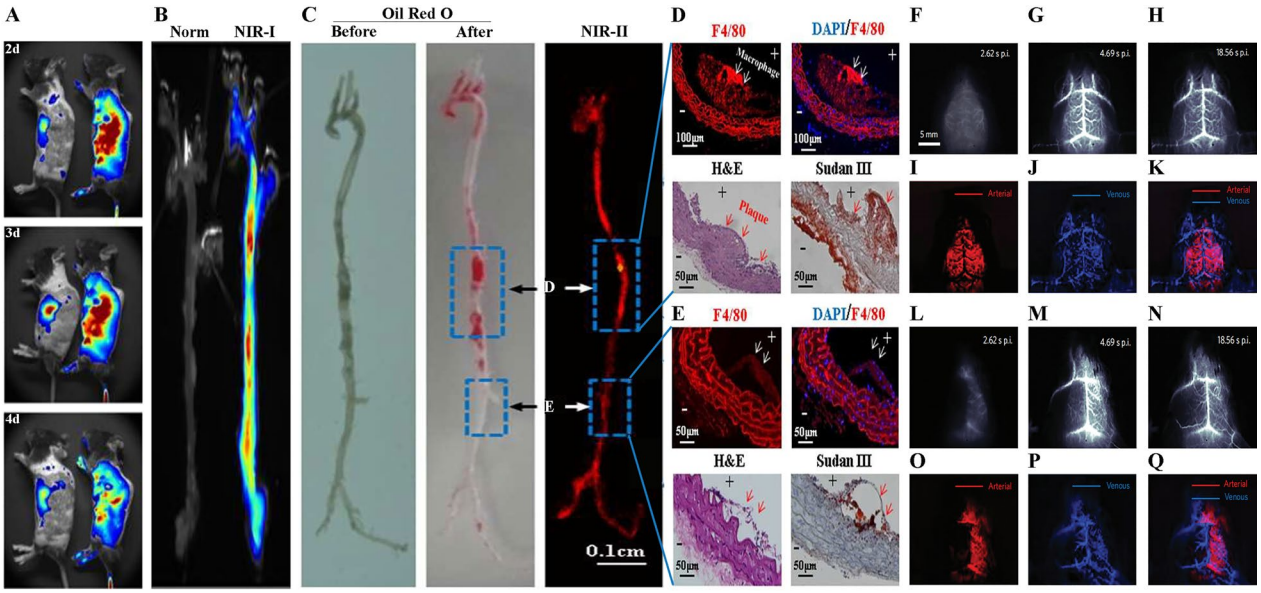

Fig. 5 Comparison of the NIR-I and NIR-II signals for AS imaging. **A** Time-based in vivo NIR-I fluorescence imaging of control and atherosclerotic animals following intravenous BOD-L-βGal-NP (300 μL, 33.3 mg/mL) injection. Reproduced from ref. [99]. **B** NIR-I fluorescence images of an atherosclerotic mouse and a control mouse aortic arch following one day of BOD-L-βGal-NP injection. Reproduced from ref. [99]. **C** Aortic fluorescence imaging using bright field and NIR-II fluorescence. After receiving an intravenous injection of ICG@PEG-Ag_2S, the aortas were removed from the ApoE−/− mice and stained using Oil Red O. Reproduced from ref. [100]. **D**, **E** H&E and immunohistochemical staining of the dissected aortas corresponding to panel A. Macrophages are shown by white arrows, while atherosclerotic plaques are indicated by red arrows. Reproduced from ref. [100]. **F**–**H** Time frame NIR-IIa images of a healthy control mouse (Mouse C1). **I**–**K** Mouse C1 venous (blue) and arterial (red) veins are depicted in superimposed PCA images. **L**–**N** Time-course NIR-IIa images of a mouse (Mouse M1) that underwent MCAO. **O**–**Q** PCA superimposed pictures of mouse M1 venous (blue) and arterial (red) veins. Reproduced from ref. [87]

fluorescence efficiency, good water solubility, and good biocompatibility.

Application of NIRF in AS imaging

Rupture or hemorrhage of advanced unstable AS plaques is the main cause of death from acute cardiovascular and cerebrovascular diseases. If the diseased area can be diagnosed and treated in the early stage of AS, the progression of AS plaques can be inhibited, and irreversible damage to the heart and brain tissues can be reduced. NIRF imaging has emerged as a powerful in vivo approach for the molecular imaging of AS [91]. In combination with NIRF molecular imaging agents, intravascular NIRF imaging is a promising new approach for imaging the biology of small-diameter arteries, such as coronary arteries, at high risk for AS and will also aid in timely diagnosis and prevention of acute cardio-cerebrovascular diseases [92, 93].

NIR-I imaging of AS

ICG is an NIRF imaging agent approved by the Food and Drug Administration (FDA) that can target macrophages and lipids in atherosclerotic plaques [94]. Johan et al. diagnosed 8 patients with carotid atherosclerotic plaque by ICG for the first time [94]. Within 2 h after intravenous injection of ICG, intravascular NIRF imaging accurately locates lesions through targeted accumulation of ICG in atherosclerotic plaques, and no adverse clinical events occur within 30 days after intravenous injection of ICG; this approach represents an important milestone in the use of NIRF imaging in atherosclerotic imaging [94]. Interestingly, intracoronary NIRF-OCT imaging with ICG probes accurately identified coronary plaques in three porcine models of AS, and ICG was spatially associated with local areas of plaque macrophages and lipids, especially intracavicular hemorrhages [94]. The ICG probe also showed excellent NIRF imaging potential in a variety of AS models. In a rabbit AS model, ICG can target coronary artery plaques within 20 min after intravenous injection [95]. Subsequent in vitro studies using human macrophages have shown that ICG will prioritize the targeting of lipid-containing macrophages [95]. Importantly, NIRF imaging of atherosclerosis by ICG probes can independently predict plaque progression in large and medium-sized arteries, such as coronary arteries. Compared with continuous IVUS, NIRF imaging can more accurately predict and quantify the magnitude of atherosclerotic plaque progression at 8 to 12 weeks ($p < 0.005$) [96]. Additionally, NIRF imaging with an ICG probe for AS can also accurately predict thrombosis in

atherosclerotic plaques. In 60 rat atherosclerotic models, 31 cases of thrombosis were detected by histology, and 29 cases were detected by NIRF imaging, for a coincidence rate of 93.5% [97]. There was a significant correlation between all the comparisons (each $p \leq 0.001$), indicating that NIRF imaging may be an important tool for detecting acute thrombosis in vascular interventional surgery [97].

NIR-II imaging of AS

Although NIR-I imaging, represented by ICG, has shown great potential in atherosclerotic plaque imaging, compared with NIR-I imaging, NIR-II imaging is more suitable for providing high-resolution intracavascular AS plaque details due to its lower spontaneous background fluorescence, greater tissue penetration and SBR. Jian Chen et al. developed the NIR-I fluorescence probe BOD-L β Gal, which can be used for in vivo imaging of atherosclerotic vessels (Fig. 5A, B) [98]. However, due to its relatively low quantum yield and tissue penetrability, its imaging applications for deep blood vessels are limited. The appearance of inorganic component probes such as QDs allows higher-resolution NIR-II imaging of atherosclerotic plaques. Chen Wu et al. prepared ICG@PEG-Ag_2S nanoprobes for in vivo imaging of atherosclerosis. NIR-II Ag_2S QDs targeting AS plaques in the aortas of ApoE.$^{-/-}$ mice can accurately identify tiny AS plaques in mice and achieve almost the same clear imaging effect as aortic oil red O staining (Fig. 5C–E) [99].

Unfortunately, most NIR-II probes previously exhibited a low photoluminescence quantum yield (PLQY) (0.009 ~ 0.235%), which led to a long exposure time and reduced imaging speed. To solve this problem, through multi-ion doping and core–shell structure design, Yongwei Guo et al. proposed the use of the lanthanide-doped nanoparticle (NP) β-$NaErF_4$: 2%Ce@$NaYbF_4$@$NaYF_4$, which has a high PLQY and tunable PL lifetime [100]. By controlling the thickness of the $NaYF_4$ inert layers, the PL lifetime at 1525 nm can be adjusted from 4.8 to 6.5 ms, which is the key to fluorescence lifetime multiplexing imaging. Additionally, for NPs with a shell thickness of 4.4 nm, the highest internal PLQY was 50.1%, which was the highest value previously reported [100]. The results showed that the combination of high-density PLQY NPs and a custom-made fluorescence lifetime imaging system can achieve fast fluorescence lifetime imaging with a high signal-to-noise ratio, thus opening up a way for visual real-time monitoring of AS [100].

In addition, due to nonspecific uptake during systemic circulation and phagocytosis clearance by the body's innate immune system, the concentration of most NIR-II contrast agents is significantly reduced during atherosclerotic plaque accumulation [101]. To solve this problem, an increasing number of studies have begun to use the body's own cell membranes (such as platelet membranes, neutrophil membranes and erythrocyte membranes) to perform biochemical modifications on NIR-II probes, effectively improving the immune escape ability and plaque-activating ability of NIR-II contrast agents [101–104]. Platelets, as a type of blood cell, contain a variety of components on their membrane surface, such as glycoprotein receptors and cell adhesion molecules; these components can be effectively used for the precise localization of atherosclerotic plaques [101]. Yun Chai et al. constructed three photoreactive NO prodrugs (RBT-NO) for use in clinical medicine by using the fluorescent dye NIR-II (RBT-NH), which has good photostability and a large Stokes shift; subsequently, a simulated platelet NO nanoprodrug system (RBT3-NO-PEG@PM) was prepared by encapsulating the platelet membrane (PM). The results showed that the nanoprodrug system could effectively locate atherosclerotic plaques by platelet membrane encapsulation, achieve NIR-II imaging under 808 nm laser irradiation, and release NO to reduce lipid accumulation in atherosclerotic plaques and improve inflammation in the lesion [101]. Finally, the visual diagnosis and treatment of atherosclerotic plaques can be performed [101]

Moreover, many studies have reported that, in contrast to previous invasive imaging methods, which require craniotomy to accurately detect deep blood vessels, NIR-II can image cerebral blood vessels more quickly, clearly and noninvasively [104, 105]. Dynamic NIR-IIa imaging of cerebral blood perfusion can accurately determine the hemodynamic differences between deep and small cerebral vessels through principal component analysis (PCA), thereby providing hemorheological information on early AS plaques (Fig. 5F-Q) [86]. Interestingly, an increasing number of studies are interested in utilizing multimodal imaging combined with NIR-II and other imaging methods to achieve accurate localization of atherosclerotic plaques in cardiovascular and cerebrovascular arteries [106, 107]. Liwei et al. combined an ASA6 antibody that actively targets human plaques with $NaNdF_4$@$NaGdF_4$ nanoparticles to achieve noninvasive imaging of atherosclerotic plaques via MRI and NIR-II imaging [107].

Exploration of macrophages targeted by NIR-I and NIR-II in AS

As the pathological basis of cardiovascular and cerebrovascular diseases, atherosclerosis is mainly driven by specific cell groups, such as macrophages and smooth muscle cells. Effective noninvasive methods are needed to assess the potential fatality risk of AS, monitor treatment results, and use near-infrared fluorescent nanomaterials to specifically identify cells or biomolecules in the

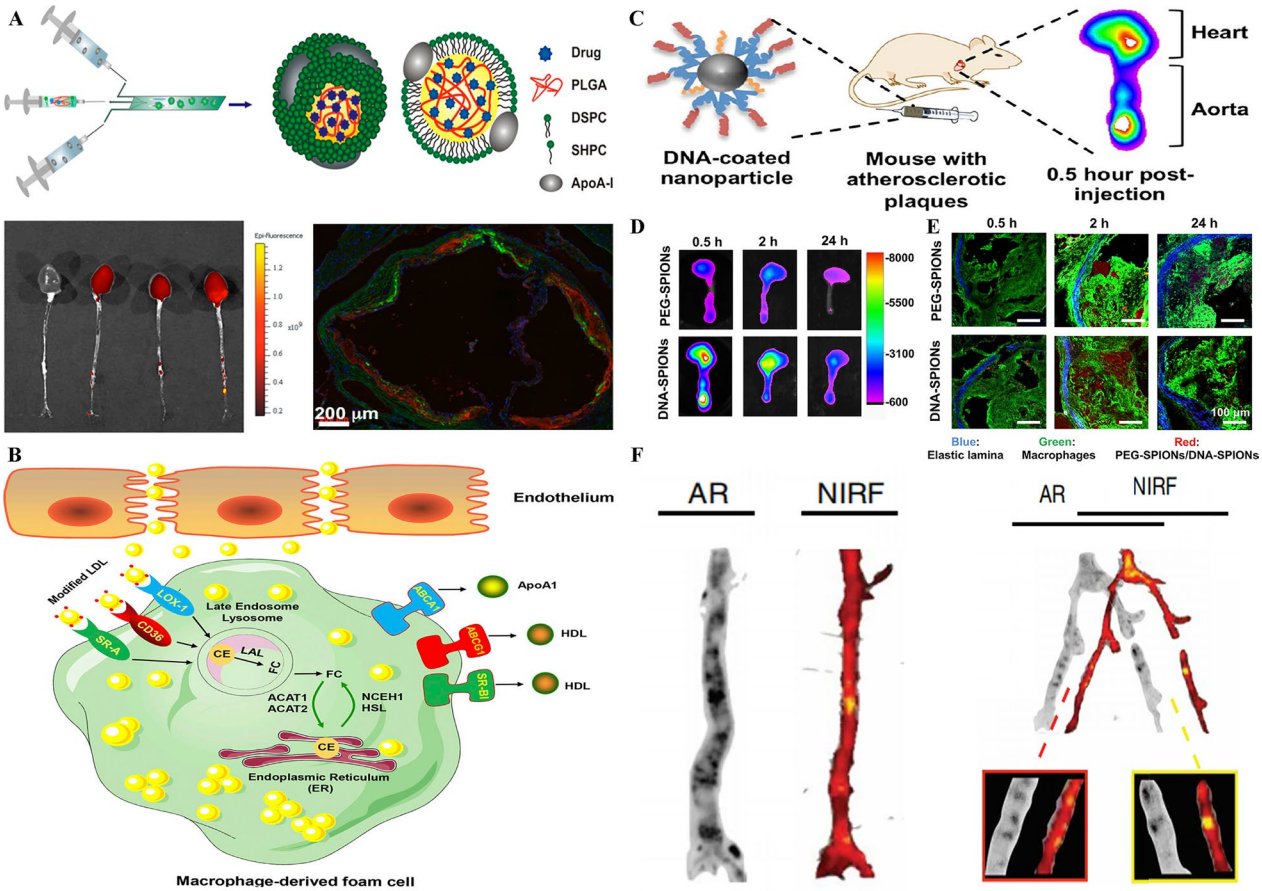

Fig. 6 Monitoring of macrophage-mediated vascular inflammation by near-infrared fluorescence imaging. **A** Schematic representation of PLGA-HDL synthesis using microfluidic technology. The mice injected with PLGA-HDL exhibited uptake in both the aortic root and the thoracic and abdominal aorta. Reproduced from ref. [121]. **B** Therapeutic targets for foam cell production by macrophages. Reproduced from ref. [125]. **C** Schematic depiction of DNA-SPIONs. Coating nanoparticles with DNA can help surgeons accurately locate atherosclerotic plaques in the aortic root. Reproduced from ref. [126]. **D** At 0.5, 2 and 24 h after injection, ex vivo NIRF images of the heart and aorta removed from ApoE−/− mice showing atherosclerotic plaques were acquired. Cy5.5-DNA-SPIONs accumulated in plaques more quickly than Cy5.5-PEG-SPIONs did. Reproduced from ref. [126, 127]. **E** The buildup of Cy5.5-DNA-SPIONs, which are more common than Cy5.5-PEG-SPIONs (both red) inside or close to plaque macrophages (green) at 0.5 and 2 h after injection, was confirmed by immunofluorescence staining of the aortic root. Reproduced from ref. [126, 127]. **F** S-HDL regional distribution in atherosclerotic samples from pigs (right) and rabbits (left) 48 h after injection, as assessed by near-infrared fluorescence (NIRF; DiD-S-HDL) and autoradiography (AR; [89Zr]-S-HDL) reproduced from ref. [128]

vascular system to target visualization drugs to early AS plaques. To date, a variety of nanomaterial systems for preclinical molecular imaging targeting AS cell populations have been developed. These markers are mainly used to detect vascular wall inflammation and evaluate subendothelial lipid accumulation [54]. Chronic inflammation triggered by lipids exacerbates the deterioration of AS, and an imbalance in M1 and M2 macrophage polarization in atherosclerotic plaques largely determines the direction of inflammation and the stability of atherosclerotic plaques. Thus, focusing on the polarization of M1 and M2 macrophages seems to be a significant way to inhibit the progression of atherosclerosis [108–111].

The role of macrophage polarization in the progression of atherosclerosis.

AS, a chronic inflammatory vascular disease, is characterized by inflammatory cell infiltration and subendothelial lipid accumulation [112]. In different microenvironments, macrophages in AS plaques can be polarized into M1 and M2 macrophages. The proportions of M1 and M2 cells determine the direction of inflammation development, the content of lipids in plaques, and the stability of plaques. Significantly, M1 macrophages are distributed mainly in the shoulder area of plaques prone to rupture, while M2 macrophages are located mainly in relatively stable areas with low lipid content far from the necrotic lipid core [113, 114].

Monitoring of macrophage-mediated vascular inflammation by near-infrared fluorescence imaging

Macrophage-mediated chronic inflammation is widely recognized as a critical factor in the development of atherosclerosis and contributes to plaque instability and an elevated risk of rupture [115]. The use of nanomaterials to target and evaluate the load of immune cells in plaques is an interesting method for evaluating plaque load and development. In the complex atherosclerotic plaque immune microenvironment, which includes macrophages, T cells and dendritic cells, macrophages are the primary target cells for molecular imaging-based plaque detection due to their major role in plaque progression [116]. To this end, different macrophage-specific ligands, including antibodies against monocytes/macrophages, have been used to modify nanoparticles.

At present, most studies mainly use the surface markers of macrophages in AS plaques as targets. Scavenger receptor A (SR-A) has become a common target of plaque macrophages because it is overexpressed in atherosclerotic activated macrophages and promotes the absorption of oxidized low-density lipoprotein (ox-LDL) [117, 118]. Based on this principle, Zhang et al. used DNA-IONPs, which can be detected by NIRF, to target the SR-A of macrophages, which can be very accurately positioned on the aortic plaque [119].

High-density lipoprotein (HDL) has the natural ability to target macrophages. Therefore, Mulder et al. constructed PLGA-HDL composite nanoparticles with high safety and selective recognition of macrophages in AS plaques. The authors connected the fluorescent dye DiR to the surface of PLGA-HDL to perform NIR-I imaging of macrophages in the AS area. Finally, vascular inflammation was evaluated by comparing the fluorescence intensity of blood vessels (Fig. 6A) [120].

To date, macrophages have been shown to play a diversified and dynamic role in immune function through different polarization phenotypes, such as the classically activated proinflammatory (M1) phenotype or the alternately activated anti-inflammatory and healing (M2) phenotype. However, an imbalance in macrophage polarization can promote the development of atherosclerosis. Therefore, the use of NIRF technology to accurately identify M1 macrophages and inhibit their polarization or promote their polarization effectively inhibits the inflammatory process in atherosclerosis. Heemin Kang et al. developed a photoresponsive nanocarrier based on upconversion nanoparticles (UCNPs), which can be used to control the level of intracellular calcium via the use of near-infrared light to regulate the polarization of macrophages. These findings suggest that the remote control of intracellular calcium elevation mediated by near-infrared light promotes M1 polarization but inhibits M2 polarization through porcine skin. In contrast, intracellular calcium depletion controlled by near-infrared light inhibited M1 polarization but encouraged macrophages to produce M2 polarization markers [121].

Evaluation of lipid accumulation in foam cells by NIRF imaging

The accumulation of lipids beneath the vascular endothelium represents a significant contributing factor to the progression of atherosclerosis. Within this context, subendothelial macrophages and vascular smooth muscle cells (VSMCs) experience an increase in lipid uptake and cholesterol esterification, leading to inadequate cholesterol efflux and the subsequent formation of foam cells. These foam cells, in turn, play a role in the recruitment of additional immune cells and the advancement of plaque development. Increased lipid absorption and cholesterol esterification coexist with inadequate cholesterol efflux in the context of atherosclerosis. This leads to an overabundance of cholesterol ester (CE), which builds up inside macrophages and ultimately produces foam cells [122, 123]. Therefore, focusing on foam cells and the uptake, esterification, and efflux pathways that are linked to them may be useful therapeutic strategies for atherosclerosis detection and management.

Therapeutic strategy of targeting macrophage-derived foam cells by NIRF imaging

Foam cells produced from macrophages constitute the primary component of the necrotic core within atherosclerotic plaques, so targeted intervention in the AS formation process guided by NIRF imaging is key for treating atherosclerosis. Following endothelial damage, LDL pierces the endothelial cell monolayer and is modified to form ox-LDL, which causes atherosclerosis. Scavenger receptors (SRs), including CD36, SR-An, and LOX-1, on the membrane of macrophages absorb ox-LDL, which is subsequently transported to the endosome/lysosome. Lysosomal acid lipase (LAL) is responsible for degrading the CE present in low-density lipoprotein particles, converting it into free cholesterol (FC) and free fatty acids. Subsequently, acyl coenzyme A: cholesterol acyltransferase-1/-2 (ACAT1 and ACAT2) can re-esterify FC in the endoplasmic reticulum (ER), leading to the accumulation of CEs and the formation of lipid droplets. Neutral cholesterol ester hydrolases (NCEHs), including NCEH1 and hormone-sensitive lipase (HSL), are responsible for hydrolyzing CEs to release FC. The liberated FC can then be transported out of macrophages by cholesterol efflux transporters such as ATP-binding cassette A1 (ABCA1), with ApoA-1 serving as a receptor; ATP-binding cassette G1 (ABCG1); and scavenger receptor class B type 1 (SR-B1), with HDL serving as a receptor (Fig. 6B) [124]. Lei

Zhang et al. conjugated DNA oligonucleotides to polyethylene glycol-coated superparamagnetic iron oxide nanoparticles (PEG-SPIONs), resulting in the formation of DNA-coated superparamagnetic iron oxide nanoparticles (DNA-SPIONs), which effectively accumulate in atherosclerotic plaques by targeting SR-A on macrophages (Fig. 6C) [125]. NIRF imaging revealed that DNA-SPIONs accumulated mainly in the heart and aortic root after injection in vivo and were absorbed mainly by aortic M2 macrophages (Fig. 6D, E) [125, 126]. Tina Binderup et al. conducted NIRF imaging studies in rabbits and pigs to assess plaque targeting and vascular wall permeability, which was achieved by developing DiD-S-HDL and [89Zr]-S-HDL nanoparticles for the purpose of the study. A comparison of the corresponding arterial samples with [89Zr]-S-HDL autoradiography revealed that DiD-S-HDL and [89Zr]-S-HDL were colocalized in the plaque (Fig. 6F) [127], indicating that the accumulation of HDL nanobiological agents in the vascular wall depends not only on the permeability of microvessels but also on their inherent affinity for macrophages [128].

Conclusion

Here, we review the latest applications of near-infrared optical nanomaterials in atherosclerotic biological imaging and summarize the benefits of fluorescent nanomaterials with NIR-1 to NIR-II for in vivo imaging. Although a series of modalities are used in these studies, NIR-I imaging is by far the most common. Considering the broad clinical application of NIR-I, broader application prospects should be developed for NIR-II fluorescence imaging, which would result in lower spontaneous background fluorescence, increased SNR and deeper tissue penetration.

Limitations and prospects

Although noninvasive NIRF imaging directed at foam cells shows promise in identifying susceptible plaques, there are still many shortcomings in evaluating the degree of lipid accumulation in foam cells by NIRF imaging at this stage. First, ASs are not imaged with clearer NIR-IIs, so it is difficult to accurately evaluate the distribution and accumulation of lipids in AS plaques. Second, the effects of M1/M2 macrophage polarization on lipid uptake, degradation and efflux in AS plaques have not yet been further explored, so it is difficult to develop multimodal nanomaterials for use with NIRF to regulate the dynamic balance of cholesterol in AS plaques. Finally, the application of NIRF imaging in AS lipid assessment has been limited mainly to preclinical studies because of the lack of binding of clinically approved NIRF probes and targeted ligands and the lack of clinical integration of NIRF imaging systems.

Under physiological conditions, the balance between lipid "inputs" and "outputs" regulates the dynamic balance of cholesterol. Foam cells are created when the equilibrium is disrupted by disease conditions (such as atherosclerosis). Consequently, three primary methods are used to decrease the production of foam cells: decrease SR-mediated lipid uptake, decrease ACAT-mediated cholesterol esterification, and increase transporter-mediated cholesterol export. An emerging strategy to actively target cells in AS plaques is to use intelligent or responsive nanomaterial probes, which can be detected by molecular imaging only after biological processes are activated. Rather than focusing on particular cell surface receptors, Ikeda et al. created an enabled NIRF probe that employs iron oxide nanoparticles coupled to indocyanine green [124]. Only after the lysosome is broken down and incorporated into macrophages via scavenger receptor-mediated uptake can the self-quenching ionic liquid ICG be activated. In a similar vein, reactive PAI nanoprobes with two NIRF reagents greatly increase macrophage absorbance to glutathione (GSH)/hydrogen peroxide (H_2O_2) redox reactions at 765 nm and 680 nm, enabling very sensitive early detection of susceptible plaques [125]. Moreover, biological nanodrug delivery systems, such as living macrophages, can be used to deliver drugs in situ to stimulate the immune system and encourage M2 macrophage polarization to inhibit the progression of AS, which is also a new idea for anti-AS immunotherapy. Recent studies have reported that PLPNPs can be used to modify the surface of bone marrow-derived macrophages (BMDMs) to construct a biomimetic system (MPLP). The biomimetic system can perform tumor-targeted delivery of PLPNPs to achieve controlled medicant release and trigger a localized immune response specific to the tumor, which eventually induces BMDMs to polarize into antitumor M1 macrophages, effectively inhibiting the growth of local and metastatic tumors. Notably, this kind of immunotherapy does not cause an adverse pathological immune reaction, which provides a new idea for antiatherosclerotic immunotherapy in the future [129].

Although significant progress has been made in the development of NIR-I to NIR-II fluorescent nanomaterials, most of the research on NIR fluorescent nanomaterials is still in the preclinical research stage because of their low biological safety and quantum yield. The toxicity and destiny of nanomaterials within the body can be primarily influenced by the modification of surface charge and functional groups, which can significantly affect the imaging speed and resolution. Therefore, improving the biological safety and quantum yield of NIR-II nanomaterials and meeting the treatment requirements for various stages of AS are highly important. We firmly believe that NIRF nanoparticles hold enormous value for the

treatment and detection of vascular disorders, including atherosclerosis, and could improve the prognosis of patients.

Acknowledgements
We appreciate the support and guidance of the Key Laboratory of Imaging Diagnosis and Minimally Invasive Intervention Research.

Author contributions
L.S., G.F.S. and Y.R.B. researched data for the article; L.S., G.F.S. and M.J.C. contributed to discussion of the content; L.S., G.F.S., W.Q.C., Y.Z. and J.Y.D. wrote the article; and J.C.Y., Y.R.B., J.S.J. and Z.W.Z. reviewed and/or edited the article before submission. We appreciate the support and guidance of the Key Laboratory of Imaging Diagnosis and Minimally Invasive Intervention Research.

Funding
This work was supported by the National Natural Science Foundation of China (8227070292 to Chenying Lu), the Key R&D Program of Lishui (2022ZDYF12 to Zhongwei Zhao) and the Exploration Project of Zhejiang Natural Science Foundation (LTGY23H180006 to Jingjing Song). The sponsors had no role in the study design, data collection, data analyses, interpretation, or writing of the manuscript.

Availability of data and materials
Not applicable.

Declarations

Ethics approval and consent to participate
Not applicable.

Consent for publication
We state that the manuscript has been read and approved by all the authors, that the requirements for authorship have been met and that each author attests that the manuscript represents honest work. We state that each author has made substantial contributions to the conception and design of the study, acquisition of data, or analysis and interpretation of data; has been involved in drafting the article or revising it critically for important intellectual content; and has approved the final version for submission.

Competing interests
The authors declare no competing interests.

Author details
[1]Key Laboratory of Imaging Diagnosis and Minimally Invasive Intervention Research, The Fifth Affiliated Hospital of Wenzhou Medical University, No 289, Kuocang Road, Lishui 323000, China. [2]Department of Interventional Radiology, The Fifth Affiliated Hospital of Wenzhou Medical University, No 289, Kuocang Road, Lishui 323000, China.

Received: 20 October 2023 Accepted: 5 July 2024
Published online: 12 August 2024

References

1. Organization GWH. World health statistics 2022: monitoring health for the SDGs, sustainable development goals. Geneva: World Health Organization; 2022.
2. Dai T, He W, Yao C, Ma X, Ren W, Mai Y, Wu A. Applications of inorganic nanoparticles in the diagnosis and therapy of atherosclerosis. Biomater Sci. 2020;8:3784–99. https://doi.org/10.1039/d0bm00196a.
3. Hoogendoorn A, Avery TD, Li J, Bursill C, Abell A, Grace PM. Emerging therapeutic applications for fumarates. Trend Pharmacol Sci. 2021;42:239–54. https://doi.org/10.1016/j.tips.2021.01.004.
4. Shen L, Li H, Chen W, Su Y, Yu J, Chen M, Shu G, Qiao E, Guo X, Xu M, et al. Integrated application of transcriptome and metabolomics reveals potential therapeutic targets for the polarization of atherosclerotic macrophages. Biochim Biophys Acta Mol Basis Dis. 2022;1868: 166550. https://doi.org/10.1016/j.bbadis.2022.166550.
5. Shen L, Chen W, Ding J, Shu G, Chen M, Zhao Z, Xia S, Ji J. The role of metabolic reprogramming of oxygen-induced macrophages in the dynamic changes of atherosclerotic plaques. Faseb j. 2023;37: e22791. https://doi.org/10.1096/fj.202201486R.
6. Adams HP Jr, Bendixen BH, Kappelle LJ, Biller J, Love BB, Gordon DL, Marsh EE 3rd. Classification of subtype of acute ischemic stroke. Definitions for use in a multicenter clinical trial. TOAST. Trial of Org 10172 in acute stroke treatment. Stroke. 1993;24:35–41. https://doi.org/10.1161/01.str.24.1.35.
7. Wright RS, Ray KK, Raal FJ, Kallend DG, Jaros M, Koenig W, Leiter LA, Landmesser U, Schwartz GG, Friedman A, et al. Pooled patient-level analysis of inclisiran trials in patients with familial hypercholesterolemia or atherosclerosis. J Am Coll Cardiol. 2021;77:1182–93. https://doi.org/10.1016/j.jacc.2020.12.058.
8. Sun B, Giddens DP, Long R Jr, Taylor WR, Weiss D, Joseph G, Vega D, Oshinski JN. Automatic plaque characterization employing quantitative and multicontrast MRI. Magn Reson Med. 2008;59:174–80. https://doi.org/10.1002/mrm.21279.
9. Zhao M, Li B, Wang P, Lu L, Zhang Z, Liu L, Wang S, Li D, Wang R, Zhang F. Supramolecularly engineered NIR-II and upconversion nanoparticles in vivo assembly and disassembly to improve bioimaging. Adv Mater. 2018;30: e1804982. https://doi.org/10.1002/adma.201804982.
10. Fabiani I, Palombo C, Caramella D, Nilsson J, De Caterina R. Imaging of the vulnerable carotid plaque: Role of imaging techniques and a research agenda. Neurology. 2020;94:922–32. https://doi.org/10.1212/wnl.0000000000009480.
11. Wang X, Lin Y, Matsumura M, Usui E, Lee T, Zhang W, Cao Y, Liu M, Hoshino M, Yonetsu T, et al. TCT-67 post-stent OCT vs IVUS predictors of 2 year outcomes. J Am Coll Cardiol. 2018;72:B29–30. https://doi.org/10.1016/j.jacc.2018.08.1157.
12. Cheng Y, Feng G, Xia J, Gasior P, Wang Q, Perkins L, Rapoza R, McGregor J, Conditt G, Kaluza G, Granada J. TCT-833 late lumen gain with bioresorbable vascular scaffold in the porcine model of spontaneous untreated atherosclerosis: a 3 year IVUS and OCT study. J Am Coll Cardiol. 2016;68:B337. https://doi.org/10.1016/j.jacc.2016.09.862.
13. Cires-Drouet RS, Mozafarian M, Ali A, Sikdar S, Lal BK. Imaging of high-risk carotid plaques: ultrasound. Semin Vasc Surg. 2017;30:44–53. https://doi.org/10.1053/j.semvascsurg.2017.04.010.
14. Bos D, van Dam-Nolen DHK, Gupta A, Saba L, Saloner D, Wasserman BA, van der Lugt A. Advances in multimodality carotid plaque imaging: AJR expert panel narrative review. AJR Am J Roentgenol. 2021;217:16–26. https://doi.org/10.2214/ajr.20.24869.
15. Hecht HS, Achenbach S, Kondo T, Narula J. High-risk plaque features on coronary CT angiography. JACC Cardiovasc Imaging. 2015;8:1336–9. https://doi.org/10.1016/j.jcmg.2014.11.018.
16. Saba L, Francone M, Bassareo PP, Lai L, Sanfilippo R, Montisci R, Suri JS, De Cecco CN, Faa G. CT attenuation analysis of carotid intraplaque hemorrhage. AJNR Am J Neuroradiol. 2018;39:131–7. https://doi.org/10.3174/ajnr.A5461.
17. Di Napoli A, Cheng SF, Gregson J, Atkinson D, Markus JE, Richards T, Brown MM, Sokolska M, Jäger HR. Arterial spin labeling MRI in carotid stenosis: arterial transit artifacts may predict symptoms. Radiology. 2020;297:652–60. https://doi.org/10.1148/radiol.2020200225.
18. Stendahl JC, Kwan JM, Pucar D, Sadeghi MM. Radiotracers to address unmet clinical needs in cardiovascular imaging, part 1: technical considerations and perfusion and neuronal imaging. J Nucl Med. 2022;63:649–58. https://doi.org/10.2967/jnumed.121.263506.
19. Meester EJ, Krenning BJ, de Swart J, Segbers M, Barrett HE, Bernsen MR, Van der Heiden K, de Jong M. Perspectives on small animal radionuclide imaging; considerations and advances in atherosclerosis. Front Med (Lausanne). 2019;6:39. https://doi.org/10.3389/fmed.2019.00039.
20. Aboyans V, Ricco JB, Bartelink MEL, Björck M, Brodmann M, Cohnert T, Collet JP, Czerny M, De Carlo M, Debus S, et al. 2017 ESC guidelines on the diagnosis and treatment of peripheral arterial diseases, in collaboration with the European society for vascular surgery (ESVS): document covering atherosclerotic disease of extracranial carotid and vertebral, mesenteric, renal, upper and lower extremity arteries endorsed by: the European stroke organization (ESO) the task force for the diagnosis and treatment of peripheral arterial diseases of the European society

of cardiology (ESC) and of the European society for vascular surgery (ESVS). Eur Heart J. 2018;39:763–816. https://doi.org/10.1093/eurheartj/ehx095.
21. McGoron AJ, Mao X, Georgiou MF, Kuluz JW. Computer phantom study of brain PET glucose metabolism imaging using a rotating SPECT/PET camera. Comput Biol Med. 2005;35:511–31. https://doi.org/10.1016/j.compbiomed.2004.03.005.
22. Scherer DJ, Shishikura D, Andrews J, Di Giovanni G, Jones S, Honda S, Butters J, Kataoka Y, Nicholls SJ. Coronary artery echo-attenuated plaques in acute coronary syndromes: a serial intravascular ultrasound imaging study. Eur Heart J. 2020. https://doi.org/10.1093/ehjci/ehaa946.1396.
23. Alfonso F, Rivero F, Sánchez-Madrid F. Variability in atherogenic lipoproteins and coronary artery disease progression. Eur Heart J. 2018;39:2559–61. https://doi.org/10.1093/eurheartj/ehy348.
24. Cao M, Zhao L, Ren X, Wu T, Yang G, Du Z, Yu H, Dai J, Li L, Wang Y, et al. Pancoronary plaque characteristics in STEMI caused by culprit plaque erosion versus rupture: 3-vessel OCT study. JACC Cardiovasc Imag. 2021;14:1235–45. https://doi.org/10.1016/j.jcmg.2020.07.047.
25. Rosenthal N, Costa MA. Unravelling the endovascular microenvironment by optical coherence tomography. Eur Heart J. 2010;31:139–42. https://doi.org/10.1093/eurheartj/ehp481.
26. Xu R, Zhao Q, Wang T, Yang Y, Luo J, Zhang X, Feng Y, Ma Y, Dmytriw AA, Yang G, et al. Optical coherence tomography in cerebrovascular disease: open up new horizons. Transl Stroke Res. 2023;14:137–45. https://doi.org/10.1007/s12975-022-01023-6.
27. Jansen K, van Soest G, van der Steen AF. Intravascular photoacoustic imaging: a new tool for vulnerable plaque identification. Ultrasound Med Biol. 2014;40:1037–48. https://doi.org/10.1016/j.ultrasmedbio.2014.01.008.
28. Wu M, Fw van der Steen A, Regar E, van Soest G. Emerging technology update intravascular photoacoustic imaging of vulnerable atherosclerotic plaque. Interv Cardiol. 2016;11:120–3. https://doi.org/10.15420/icr.2016:13:3.
29. Liu H, Hong G, Luo Z, Chen J, Chang J, Gong M, He H, Yang J, Yuan X, Li L, et al. Atomic-precision gold clusters for NIR-II imaging. Adv Mater. 2019;31: e1901015. https://doi.org/10.1002/adma.201901015.
30. Liu C, Wang X, Liu J, Yue Q, Chen S, Lam J, Luo L, Tang B. Near-infrared AIE dots with chemiluminescence for deep-tissue imaging. Adv Mater. 2020;32: e2004685. https://doi.org/10.1002/adma.202004685.
31. Li L, Shao C, Liu T, Chao Z, Chen H, Xiao F, He H, Wei Z, Zhu Y, Wang H, et al. An NIR-II-emissive photosensitizer for hypoxia-tolerant photodynamic theranostics. Adv Mater. 2020;32: e2003471. https://doi.org/10.1002/adma.202003471.
32. Abdel Jaleel GA, Azab SS, El-Bakly WM, Hassan A. 'Methyl palmitate attenuates adjuvant induced arthritis in rats by decrease of CD68 synovial macrophages. Biomed Pharmacother. 2021;137: 111347. https://doi.org/10.1016/j.biopha.2021.111347.
33. Xu C, Jiang Y, Han Y, Pu K, Zhang R. A polymer multicellular nanoengager for synergistic NIR-II photothermal immunotherapy. Adv Mater. 2021;33: e2008061. https://doi.org/10.1002/adma.202008061.
34. Wu M, Li X, Guo Q, Li J, Xu G, Li G, Wang J, Zhang X. Magnetic mesoporous silica nanoparticles-aided dual MR/NIRF imaging to identify macrophage enrichment in atherosclerotic plaques. Nanomedicine. 2021;32: 102330. https://doi.org/10.1016/j.nano.2020.102330.
35. Horvath M, Hajek P, Stechovsky C, Honek J, Spacek M, Veselka J. The role of near-infrared spectroscopy in the detection of vulnerable atherosclerotic plaques. Arch Med Sci. 2016;12:1308–16. https://doi.org/10.5114/aoms.2016.62904.
36. Stone GW, Maehara A, Lansky AJ, de Bruyne B, Cristea E, Mintz GS, Mehran R, McPherson J, Farhat N, Marso SP, et al. A prospective natural-history study of coronary atherosclerosis. N Engl J Med. 2011;364:226–35. https://doi.org/10.1056/NEJMoa1002358.
37. Ughi GJ, Wang H, Gerbaud E, Gardecki JA, Fard AM, Hamidi E, Vacas-Jacques P, Rosenberg M, Jaffer FA, Tearney GJ. Clinical characterization of coronary atherosclerosis with dual-modality OCT and near-infrared autofluorescence imaging. JACC Cardiovasc Imaging. 2016;9:1304–14. https://doi.org/10.1016/j.jcmg.2015.11.020.
38. Prati F, Romagnoli E, Burzotta F, Limbruno U, Gatto L, La Manna A, Versaci F, Marco V, Di Vito L, Imola F, et al. Clinical impact of OCT findings during PCI: The CLI-OPCI II study. JACC Cardiovasc Imaging. 2015;8:1297–305. https://doi.org/10.1016/j.jcmg.2015.08.013.
39. Matsumoto Y. European society of cardiology (ESC) congress report from Amsterdam 2013. Circ J. 2013;77:2687–90. https://doi.org/10.1253/circj.cj-13-1213.
40. Kastrati A, Baldus S, Cremer J, Falk V, Hamm CW, Neumann FJ, Schunkert H, Welz A. Kommentar zu den "2014 ESC/EACTS guidelines on myocardial revascularization" der European society of cardiology (ESC) und der European association for cardio-thoracic surgery (EACTS). Kardiologe. 2016;10:359–70. https://doi.org/10.1007/s12181-016-0106-0.
41. Wijns W, Shite J, Jones MR, Lee SW, Price MJ, Fabbiocchi F, Barbato E, Akasaka T, Bezerra H, Holmes D. Optical coherence tomography imaging during percutaneous coronary intervention impacts physician decision-making: ILUMIEN I study. Eur Heart J. 2015;36:3346–55. https://doi.org/10.1093/eurheartj/ehv367.
42. Maehara A, Ben-Yehuda O, Ali Z, Wijns W, Bezerra HG, Shite J, Généreux P, Nichols M, Jenkins P, Witzenbichler B, Mintz GS, Stone GW. Comparison of stent expansion guided by optical coherence tomography versus intravascular ultrasound: The ILUMIEN II study (observational study of optical coherence tomography [OCT] in patients undergoing fractional flow reserve [FFR] and percutaneous coronary intervention). JACC Cardiovasc Interv. 2015;8:1704–14. https://doi.org/10.1016/j.jcin.2015.07.024.
43. Finn AV, Nakano M, Narula J, Kolodgie FD, Virmani R. Concept of vulnerable/unstable plaque. Arterioscler Thromb Vasc Biol. 2010;30:1282–92. https://doi.org/10.1161/atvbaha.108.179739.
44. Osborn EA, Kessinger CW, Tawakol A, Jaffer FA. Metabolic and molecular imaging of atherosclerosis and venous thromboembolism. J Nucl Med. 2017;58:871–7. https://doi.org/10.2967/jnumed.116.182873.
45. Varasteh Z, Hyafil F, Anizan N, Diallo D, Aid-Launais R, Mohanta S, Li Y, Braeuer M, Steiger K, Vigne J, et al. Targeting mannose receptor expression on macrophages in atherosclerotic plaques of apolipoprotein E-knockout mice using (111) in-tilmanocept. EJNMMI Res. 2017;7:40. https://doi.org/10.1186/s13550-017-0287-y.
46. MacRitchie N, Grassia G, Noonan J, Garside P, Graham D, Maffia P. Molecular imaging of atherosclerosis: spotlight on Raman spectroscopy and surface-enhanced Raman scattering. Heart. 2018;104:460–7. https://doi.org/10.1136/heartjnl-2017-311447.
47. Narita Y, Shimizu K, Ikemoto K, Uchino R, Kosugi M, Maess MB, Magata Y, Oku N, Ogawa M. Macrophage-targeted, enzyme-triggered fluorescence switch-on system for detection of embolism-vulnerable atherosclerotic plaques. J Control Releas. 2019;302:105–15. https://doi.org/10.1016/j.jconrel.2019.03.025.
48. Ehara S, Matsumoto K, Shimada K. The clinical value of high-intensity signals on the coronary atherosclerotic plaques: noncontrast T1-weighted magnetic resonance imaging. Int J Mol Sci. 2016. https://doi.org/10.3390/ijms17071187.
49. Morf C, Sartoretti T, Gennari AG, Maurer A, Skawran S, Giannopoulos AA, Sartoretti E, Schwyzer M, Curioni-Fontecedro A, Gebhard C, et al. Diagnostic value of fully automated artificial intelligence powered coronary artery calcium scoring from 18F-FDG PET/CT. Diagnostics. 2022. https://doi.org/10.3390/diagnostics12081876.
50. Saam T, Rominger A, Wolpers S, Cyran CC, Bartenstein P, Reiser MF, Hacker M, Nikolaou K. Abstract 5814: increased arterial 18F-FDG-uptake is associated with future cardio- and cerebrovascular events: initial results of a PET-CT study considering age and cardiovascular risk factors. Circulation. 2008. https://doi.org/10.1161/circ.118.suppl_18.S_109.
51. Villena García AC, Cardo AG, Hidalgo CM, Palomo L, Lillo E, Espíldora J, Trigo JM, Chaparro MÁS, Valdivielso P. 18FDG PET/CT & arterial inflammation: predicting cardiovascular events in lung cancer. QJM. 2019;112:401–7. https://doi.org/10.1093/qjmed/hcz036.
52. Kabbany M, Joshi A, Ahlman M, Rodante J, Lerman J, Aberra T, Silverman J, Dahiya A, Bluemke D, Playford M, Mehta N. Determinants of vascular inflammation by 18-fluorodeoxyglucose Pet/Mri: findings from the psoriasis, atherosclerosis and cardiometabolic disease initiative. J Investig Med. 2016;64:815–6. https://doi.org/10.1136/jim-2016-000080.37.
53. Park CH, Givens RS. New photoactivated protecting groups. 6. p-hydroxyphenacyl: a phototrigger for chemical and biochemical probes 1,2. J Am Chem Soc. 1997;119:2453–63. https://doi.org/10.1021/ja9635589.

54. Hu J, Ortgies DH, Martín Rodríguez E, Rivero F, Aguilar Torres R, Alfonso F, Fernández N, Carreño-Tarragona G, Monge L, Sanz-Rodriguez F, et al. Optical nanoparticles for cardiovascular imaging. Adv Opt Mater. 2018;6:1800626. https://doi.org/10.1002/adom.201800626.
55. Hemmer E, Acosta-Mora P, Méndez-Ramos J, Fischer S. Optical nanoprobes for biomedical applications: shining a light on upconverting and near-infrared emitting nanoparticles for imaging, thermal sensing, and photodynamic therapy. J Mater Chem B. 2017;5:4365–92. https://doi.org/10.1039/c7tb00403f.
56. Deng X, Liang S, Cai X, Huang S, Cheng Z, Shi Y, Pang M, Ma P, Lin J. Yolk-shell structured au nanostar@metal-organic framework for synergistic chemo-photothermal therapy in the second near-infrared window. Nano Lett. 2019;19:6772–80. https://doi.org/10.1021/acs.nanolett.9b01716.
57. Cho SS, Salinas R, De Ravin E, Teng CW, Li C, Abdullah KG, Buch L, Hussain J, Ahmed F, Dorsey J, et al. Near-infrared imaging with second-window indocyanine green in newly diagnosed high-grade gliomas predicts gadolinium enhancement on postoperative magnetic resonance imaging. Mol Imag Biol. 2020;22:1427–37. https://doi.org/10.1007/s11307-019-01455-x.
58. Lin E, Alessio A. What are the basic concepts of temporal, contrast, and spatial resolution in cardiac CT? J Cardiovasc Comput Tomogr. 2009;3:403–8. https://doi.org/10.1016/j.jcct.2009.07.003.
59. Tearney GJ, Bouma BE. Atherosclerotic plaque characterization by spatial and temporal speckle pattern analysis. Opt Lett. 2002;27:533–5. https://doi.org/10.1364/ol.27.000533.
60. Lobatto ME, Fuster V, Fayad ZA, Mulder WJ. Perspectives and opportunities for nanomedicine in the management of atherosclerosis. Nat Rev Drug Discov. 2011;10:835–52. https://doi.org/10.1038/nrd3578.
61. Mulder WJ, Jaffer FA, Fayad ZA, Nahrendorf M. Imaging and nanomedicine in inflammatory atherosclerosis. Sci Transl Med. 2014. https://doi.org/10.1126/scitranslmed.3005101.
62. Hong G, Lee JC, Robinson JT, Raaz U, Xie L, Huang NF, Cooke JP, Dai H. Multifunctional in vivo vascular imaging using near-infrared II fluorescence. Nat Med. 2012;18:1841–6. https://doi.org/10.1038/nm.2995.
63. Smith AM, Mancini MC, Nie S. Bioimaging: second window for in vivo imaging. Nat Nanotechnol. 2009;4:710–1. https://doi.org/10.1038/nnano.2009.326.
64. Bashkatov AN, Genina EA, Kochubey VI, Tuchin VV. Optical properties of human skin, subcutaneous and mucous tissues in the wavelength range from 400 to 2000 nm. J Phys D Appl Phys. 2005;38:2543. https://doi.org/10.1088/0022-3727/38/15/004.
65. Fang Y, Shang J, Liu D, Shi W, Li X, Ma H. Design, synthesis, and application of a small molecular NIR-II fluorophore with maximal emission beyond 1200 nm. J Am Chem Soc. 2020;142:15271–5. https://doi.org/10.1021/jacs.0c08187.
66. Yang S, Zhang J, Zhang Z, Zhang R, Ou X, Xu W, Kang M, Li X, Yan D, Kwok RTK, et al. More is better: dual-acceptor engineering for constructing second near-infrared aggregation-induced emission luminogens to boost multimodal phototheranostics. J Am Chem Soc. 2023;145:22776–87. https://doi.org/10.1021/jacs.3c08627.
67. Ma H, Liu C, Hu Z, Yu P, Zhu X, Ma R, Sun Z, Zhang C-H, Sun H, Zhu S, Liang Y. Propylenedioxy thiophene donor to achieve NIR-II molecular fluorophores with enhanced brightness. Chem Mater. 2020;32:2061–9. https://doi.org/10.1021/acs.chemmater.9b05159.
68. Liu S, Ou H, Li Y, Zhang H, Liu J, Lu X, Kwok RTK, Lam JWY, Ding D, Tang BZ. Planar and twisted molecular structure leads to the high brightness of semiconducting polymer nanoparticles for NIR-IIa fluorescence imaging. J Am Chem Soc. 2020;142:15146–56. https://doi.org/10.1021/jacs.0c07193.
69. Sun Y, Qu C, Chen H, He M, Tang C, Shou K, Hong S, Yang M, Jiang Y, Ding B, et al. Novel benzo-bis (1,2,5-thiadiazole) fluorophores for in vivo NIR-II imaging of cancer. Chem Sci. 2016;7:6203–7. https://doi.org/10.1039/c6sc01561a.
70. Zhu S, Hu Z, Tian R, Yung BC, Yang Q, Zhao S, Kiesewetter DO, Niu G, Sun H, Antaris AL, Chen X. Repurposing cyanine NIR-I dyes accelerates clinical translation of near-infrared-II (NIR-II) bioimaging. Adv Mater. 2018. https://doi.org/10.1002/adma.201802546.
71. Ding F, Fan Y, Sun Y, Zhang F. Beyond 1000 nm emission wavelength: recent advances in organic and inorganic emitters for deep-tissue molecular imaging. Adv Healthc Mater. 2019;8: e1900260. https://doi.org/10.1002/adhm.201900260.
72. Tian R, Zeng Q, Zhu S, Lau J, Chandra S, Ertsey R, Hettie KS, Teraphongphom T, Hu Z, Niu G, et al. Albumin-chaperoned cyanine dye yields superbright NIR-II fluorophore with enhanced pharmacokinetics. Sci Adv. 2019. https://doi.org/10.1126/sciadv.aaw0672.
73. Starosolski Z, Bhavane R, Ghaghada KB, Vasudevan SA, Kaay A, Annapragada A. Indocyanine green fluorescence in second near-infrared (NIR-II) window. PLoS ONE. 2017;12: e0187563. https://doi.org/10.1371/journal.pone.0187563.
74. Godard A, Kalot G, Pliquett J, Busser B, Le Guével X, Wegner KD, Resch-Genger U, Rousselin Y, Coll JL, Denat F, et al. Water-soluble Aza-BODIPYs: biocompatible organic dyes for high contrast in vivo NIR-II imaging. Bioconjug Chem. 2020;31:1088–92. https://doi.org/10.1021/acs.bioconjchem.0c00175.
75. Bai L, Sun P, Liu Y, Zhang H, Hu W, Zhang W, Liu Z, Fan Q, Li L, Huang W. Novel aza-BODIPY based small molecular NIR-II fluorophores for in vivo imaging. Chem Commun (Camb). 2019;55:10920–3. https://doi.org/10.1039/c9cc03378e.
76. Ni Y, Lee S, Son M, Aratani N, Ishida M, Samanta A, Yamada H, Chang YT, Furuta H, Kim D, Wu J. A diradical approach towards BODIPY-based dyes with intense near-infrared absorption around λ=1100 nm. Angew Chem Int Ed Engl. 2016;55:2815–9. https://doi.org/10.1002/anie.201511151.
77. Welsher K, Liu Z, Sherlock SP, Robinson JT, Chen Z, Daranciang D, Dai H. A route to brightly fluorescent carbon nanotubes for near-infrared imaging in mice. Nat Nanotechnol. 2009;4:773–80. https://doi.org/10.1038/nnano.2009.294.
78. Yang Y, Zhang F. Molecular fluorophores for in vivo bioimaging in the second near-infrared window. Eur J Nucl Med Mol Imag. 2022;49:3226–46. https://doi.org/10.1007/s00259-022-05688-x.
79. Du Y, Xu B, Fu T, Cai M, Li F, Zhang Y, Wang Q. Near-infrared photoluminescent Ag2S quantum dots from a single source precursor. J Am Chem Soc. 2010;132:1470–1. https://doi.org/10.1021/ja909490r.
80. Yarema M, Pichler S, Sytnyk M, Seyrkammer R, Lechner RT, Fritz-Popovski G, Jarzab D, Szendrei K, Resel R, Korovyanko O, et al. Infrared emitting and photoconducting colloidal silver chalcogenide nanocrystal quantum dots from a silylamide-promoted synthesis. ACS Nano. 2011;5:3758–65. https://doi.org/10.1021/nn2001118.
81. Shen S, Wang Q. Rational tuning the optical properties of metal sulfide nanocrystals and their applications. Chem Mater. 2013;25:1166–78. https://doi.org/10.1021/cm302482d.
82. Zhao J, Zhong D, Zhou S. NIR-I-to-NIR-II fluorescent nanomaterials for biomedical imaging and cancer therapy. J Mater Chem B. 2018;6:349–65. https://doi.org/10.1039/C7TB02573D.
83. Li C, Zhang Y, Wang M, Zhang Y, Chen G, Li L, Wu D, Wang Q. In vivo real-time visualization of tissue blood flow and angiogenesis using Ag2S quantum dots in the NIR-II window. Biomaterials. 2014;35:393–400. https://doi.org/10.1016/j.biomaterials.2013.10.010.
84. Dong B, Li C, Chen G, Zhang Y, Zhang Y, Deng M, Wang Q. Facile synthesis of highly photoluminescent Ag2Se quantum dots as a new fluorescent probe in the second near-infrared window for in vivo imaging. Chem Mater. 2013;25:2503–9. https://doi.org/10.1021/cm400812v.
85. Gong H, Peng R, Liu Z. Carbon nanotubes for biomedical imaging: the recent advances. Adv Drug Deliv Rev. 2013;65:1951–63. https://doi.org/10.1016/j.addr.2013.10.002.
86. Hong G, Diao S, Chang J, Antaris AL, Chen C, Zhang B, Zhao S, Atochin DN, Huang PL, Andreasson KI, Kuo CJ, Dai H. Through-skull fluorescence imaging of the brain in a new near-infrared window. Nat Photonics. 2014;8:723–30. https://doi.org/10.1038/nphoton.2014.166.
87. Diao S, Blackburn JL, Hong G, Antaris AL, Chang J, Wu JZ, Zhang B, Cheng K, Kuo CJ, Dai H. Fluorescence imaging in vivo at wavelengths beyond 1500 nm. Angew Chem Int Ed Engl. 2015;54:14758–62. https://doi.org/10.1002/anie.201507473.
88. Wan H, Yue J, Zhu S, Uno T, Zhang X, Yang Q, Yu K, Hong G, Wang J, Li L, et al. A bright organic NIR-II nanofluorophore for three-dimensional imaging into biological tissues. Nat Commun. 2018;9:1171. https://doi.org/10.1038/s41467-018-03505-4.
89. Wu W, Yang YQ, Yang Y, Yang YM, Wang H, Zhang KY, Guo L, Ge HF, Liu J, Feng H. An organic NIR-II nanofluorophore with aggregation-induced

emission characteristics for in vivo fluorescence imaging. Int J Nanomed. 2019;14:3571–82. https://doi.org/10.2147/ijn.S198587.
90. Schaafsma BE, Verbeek FP, van der Vorst JR, Hutteman M, Kuppen PJ, Frangioni JV, van de Velde CJ, Vahrmeijer AL. Ex vivo sentinel node mapping in colon cancer combining blue dye staining and fluorescence imaging. J Surg Res. 2013;183:253–7. https://doi.org/10.1016/j.jss.2013.01.003.
91. Song JW, Ahn JW, Lee MW, Kim HJ, Kang DO, Kim RH, Kang UG, Kim YH, Han J, Park YH, et al. Targeted theranostic photoactivation on atherosclerosis. J Nanobiotechnol. 2021;19:338. https://doi.org/10.1186/s12951-021-01084-z.
92. Chowdhury MM, Piao Z, Albaghdadi MS, Coughlin PA, Rudd JHF, Tearney GJ, Jaffer FA. Intravascular fluorescence molecular imaging of atherosclerosis. Method Mol Biol. 2022;2419:853–72. https://doi.org/10.1007/978-1-0716-1924-7_52.
93. Bourantas CV, Jaffer FA, Gijsen FJ, van Soest G, Madden SP, Courtney BK, Fard AM, Tenekecioglu E, Zeng Y, van der Steen AFW, et al. Hybrid intravascular imaging: recent advances, technical considerations, and current applications in the study of plaque pathophysiology. Eur Heart J. 2017;38:400–12. https://doi.org/10.1093/eurheartj/ehw097.
94. Verjans JW, Osborn EA, Ughi GJ, Calfon Press MA, Hamidi E, Antoniadis AP, Papafaklis MI, Conrad MF, Libby P, Stone PH, et al. Targeted near-infrared fluorescence imaging of atherosclerosis: clinical and intracoronary evaluation of indocyanine green. JACC Cardiovasc Imag. 2016;9:1087–95. https://doi.org/10.1016/j.jcmg.2016.01.034.
95. Vinegoni C, Botnaru I, Aikawa E, Calfon MA, Iwamoto Y, Folco EJ, Ntziachristos V, Weissleder R, Libby P, Jaffer FA. Indocyanine green enables near-infrared fluorescence imaging of lipid-rich, inflamed atherosclerotic plaques. Sci Transl Med. 2011. https://doi.org/10.1126/scitranslmed.3001577.
96. Osborn EA, Ughi GJ, Verjans JW, Gerbaud E, Takx RA, Tawakol A, Tearney GJ, Jaffer FA. Abstract 656: in vivo plaque inflammation and endothelial permeability independently predict atherosclerosis progression: a serial multimodality imaging study. Arterioscler Thromb Vasc Biol. 2016. https://doi.org/10.1161/atvb.36.suppl_1.656.
97. Mücke T, Wolff C, Fichter AM, von Düring M, Kanatas A, Ritschl LM. Detection of thrombosis in microvessels with indocyanine green videoangiography. Br J Oral Maxillofac Surg. 2018;56:678–83. https://doi.org/10.1016/j.bjoms.2018.07.005.
98. Osborn EA, Ughi GJ, Verjans JW, Gerbaud E, Takx RA, Tawakol A, Tearney GJ, Jaffer FA. Abstract 656: in vivo plaque inflammation and endothelial permeability independently predict atherosclerosis progression: a serial multimodality imaging study. Arterioscler Thromb Vascul Biol. 2016;36:A656–A656.
99. Chen JA, Guo W, Wang Z, Sun N, Pan H, Tan J, Ouyang Z, Fu W, Wang Y, Hu W, Gu X. In vivo imaging of senescent vascular cells in atherosclerotic mice using a β-galactosidase-activatable nanoprobe. Anal Chem. 2020;92:12613–21. https://doi.org/10.1021/acs.analchem.0c02670.
100. Guo Y, Hu J, Wang P, Yang H, Liang S, Chen D, Xu K, Huang Y, Wang Q, Liu X, Zhu H. In vivo NIR-II fluorescence lifetime imaging of whole-body vascular using high quantum yield lanthanide-doped nanoparticles. Small. 2023;19: e2300392. https://doi.org/10.1002/smll.202300392.
101. Chai Y, Shangguan L, Yu H, Sun Y, Huang X, Zhu Y, Wang HY, Liu Y. Near infrared light-activatable platelet-mimicking NIR-II NO nanoprodrug for precise atherosclerosis theranostics. Adv Sci. 2023. https://doi.org/10.1002/advs.202304994.
102. Jiang ZZ, Geng XR, Su LL, Chen AN, Sheng ZH, Jiang TA. Neutrophil membrane camouflaged nanoprobes for NIR-II fluorescence imaging of inflamed, high-risk atherosclerotic plaques in mouse and rabbit models. Mater Today Chem. 2022;26: 101062. https://doi.org/10.1016/j.mtchem.2022.101062.
103. Liu B, Han G-M, Wang D-X, Liu D-B, Liu A-A, Wang J, Xiao Y-L, Yuan L, Kong D-M. Red blood cell membrane biomimetic nanoprobes for ratiometric imaging of reactive oxygen species level in atherosclerosis. Chem Eng J. 2024;479: 147515. https://doi.org/10.1016/j.cej.2023.147515.
104. Liu Y, Hanley T, Chen H, Long SR, Gambhir SS, Cheng Z, Wu JC, Fakhri GE, Anvari B, Zaman RT. Non-invasive photoacoustic imaging of in vivo mice with erythrocyte derived optical nanoparticles to detect CAD/MI. Sci Rep. 2020;10:5983. https://doi.org/10.1038/s41598-020-62868-1.
105. Welsher K, Sherlock SP, Dai H. Deep-tissue anatomical imaging of mice using carbon nanotube fluorophores in the second near-infrared window. Proc Natl Acad Sci U S A. 2011;108:8943–8. https://doi.org/10.1073/pnas.1014501108.
106. Wang S, Li X, Chong SY, Wang X, Chen H, Chen C, Ng LG, Wang JW, Liu B. In vivo three-photon imaging of lipids using ultrabright fluorogens with aggregation-induced emission. Adv Mater. 2021;33: e2007490. https://doi.org/10.1002/adma.202007490.
107. Zhang L, Xue S, Ren F, Huang S, Zhou R, Wang Y, Zhou C, Li Z. An atherosclerotic plaque-targeted single-chain antibody for MR/NIR-II imaging of atherosclerosis and anti-atherosclerosis therapy. J Nanobiotechnol. 2021;19:296. https://doi.org/10.1186/s12951-021-01047-4.
108. Moore K, Tabas IJC. Macrophages in the pathogenesis of atherosclerosis. Cell. 2011;145:341–55. https://doi.org/10.1016/j.cell.2011.04.005.
109. Swirski F, Nahrendorf MJS. Leukocyte behavior in atherosclerosis, myocardial infarction, and heart failure. Science. 2013;339:161–6. https://doi.org/10.1126/science.1230719.
110. Tabas I, Glass CJS. Anti-inflammatory therapy in chronic disease: challenges and opportunities. Science. 2013;339:166–72. https://doi.org/10.1126/science.1230720.
111. Stone G, Maehara A, Lansky A, de Bruyne B, Cristea E, Mintz G, Mehran R, McPherson J, Farhat N, Marso S, et al. A prospective natural-history study of coronary atherosclerosis. New Engl J Med. 2011. https://doi.org/10.1056/NEJMoa1002358.
112. Tabas I, Bornfeldt KJCr. Macrophage phenotype and function in different stages of atherosclerosis. Circul Res. 2016;2016(118):653–67.
113. Colin S, Chinetti-Gbaguidi G, Staels BJTr. Macrophage phenotypes in atherosclerosis. Immunol Rev. 2014;262:153–66. https://doi.org/10.1111/imr.12218.
114. Gentek R, Molawi K, Sieweke MJIr. Tissue macrophage identity and self-renewal. Immunol Rev. 2014;262:56–73. https://doi.org/10.1111/imr.12224.
115. Ye M, Zhou J, Zhong Y, Xu J, Hou J, Wang X, Wang Z, Guo D. SR-A-targeted phase-transition nanoparticles for the detection and treatment of atherosclerotic vulnerable plaques. ACS Appl Mater Interfac. 2019;11:9702–15. https://doi.org/10.1021/acsami.8b18190.
116. Zhang L, Tian XY, Chan CKW, Bai Q, Cheng CK, Chen FM, Cheung MSH, Yin B, Yang H, Yung WY, et al. Promoting the delivery of nanoparticles to atherosclerotic plaques by DNA coating. ACS Appl Mater Interfaces. 2019;11:13888–904. https://doi.org/10.1021/acsami.8b17928.
117. Sanchez-Gaytan BL, Fay F, Lobatto ME, Tang J, Ouimet M, Kim Y, van der Staay SE, van Rijs SM, Priem B, Zhang L, et al. HDL-mimetic PLGA nanoparticle to target atherosclerosis plaque macrophages. Bioconjug Chem. 2015;26:443–51. https://doi.org/10.1021/bc500517k.
118. Kang H, Zhang K, Wong DSH, Han F, Li B, Bian L. Near-infrared light-controlled regulation of intracellular calcium to modulate macrophage polarization. Biomaterials. 2018;178:681–96. https://doi.org/10.1016/j.biomaterials.2018.03.007.
119. Chistiakov DA, Melnichenko AA, Myasoedova VA, Grechko AV, Orekhov AN. Mechanisms of foam cell formation in atherosclerosis. J Mol Med. 2017;95:1153–65. https://doi.org/10.1007/s00109-017-1575-8.
120. Maguire EM, Pearce SWA, Xiao Q. Foam cell formation: a new target for fighting atherosclerosis and cardiovascular disease. Vascul Pharmacol. 2019;112:54–71. https://doi.org/10.1016/j.vph.2018.08.002.
121. Wang D, Yang Y, Lei Y, Tzvetkov NT, Liu X, Yeung AWK, Xu S, Atanasov AG. Targeting foam cell formation in atherosclerosis: therapeutic potential of natural products. Pharmacol Rev. 2019;71:596–670. https://doi.org/10.1124/pr.118.017178.
122. Binderup T, Duivenvoorden R, Fay F, van Leent MMT, Malkus J, Baxter S, Ishino S, Zhao Y, Sanchez-Gaytan B, Teunissen AJP, et al. Imaging-assisted nanoimmunotherapy for atherosclerosis in multiple species. Sci Transl Med. 2019. https://doi.org/10.1126/scitranslmed.aaw7736.
123. Pérez-Medina C, Binderup T, Lobatto ME, Tang J, Calcagno C, Giesen L, Wessel CH, Witjes J, Ishino S, Baxter S, et al. In vivo PET imaging of HDL in multiple atherosclerosis models. JACC Cardiovascular Imag. 2016;9:950–61. https://doi.org/10.1016/j.jcmg.2016.01.020.
124. Ikeda H, Ishii A, Sano K, Chihara H, Arai D, Abekura Y, Nishi H, Ono M, Saji H, Miyamoto S. Activatable fluorescence imaging of macrophages in atherosclerotic plaques using iron oxide nanoparticles conjugated with

indocyanine green. Atherosclerosis. 2018;275:1–10. https://doi.org/10.1016/j.atherosclerosis.2018.05.028.
125. Gao W, Li X, Liu Z, Fu W, Sun Y, Cao W, Tong L, Tang B. A redox-responsive self-assembled nanoprobe for photoacoustic inflammation imaging to assess atherosclerotic plaque vulnerability. Anal Chem. 2019;91:1150–6. https://doi.org/10.1021/acs.analchem.8b04912.
126. Zhou H, He H, Liang R, Pan H, Chen Z, Deng G, Zhang S, Ma Y, Liu L, Cai L. In situ poly I: C released from living cell drug nanocarriers for macrophage-mediated antitumor immunotherapy. Biomaterials. 2021;269:120670. https://doi.org/10.1016/j.biomaterials.2021.120670.
127. Staub D, Schinkel AF, Coll B, Coli S, van der Steen AF, Reed JD, Krueger C, Thomenius KE, Adam D, Sijbrands EJ, ten Cate FJ, Feinstein SB. Contrast-enhanced ultrasound imaging of the vasa vasorum: from early atherosclerosis to the identification of unstable plaques. JACC Cardiovasc Imag. 2010;3:761–71. https://doi.org/10.1016/j.jcmg.2010.02.007.
128. Li J, Li X, Mohar D, Raney A, Jing J, Zhang J, Johnston A, Liang S, Ma T, Shung KK, et al. Integrated IVUS-OCT for real-time imaging of coronary atherosclerosis. JACC Cardiovasc Imaging. 2014;7:101–3. https://doi.org/10.1016/j.jcmg.2013.07.012.
129. Zhou H, He H, Liang R, Pan H, Chen Z, Deng G, Zhang S, Ma Y, Liu L, Cai LJB. In situ poly I: C released from living cell drug nanocarriers for macrophage-mediated antitumor immunotherapy. Biomaterials. 2021. https://doi.org/10.1016/j.biomaterials.2021.120670.

Publisher's Note